Animal Shapes, Modal Analysis, and Visualization of Motion (I): Horse and Camel

Goong Chen[1,2,3] · Jingtong Huang[1] · Chunqiu Wei[4] · Jing Yang[5] ·
Matthew M. Scully[1] · Alexey Sergeev[1] · Ming-Chieh Chen[6] ·
Steven G. Krantz[7] · Pengfei Yao[8,9] · Tiexin Guo[10] · Junmin Wang[5]

Abstract

Eigenfunctions and eigenvalues of physical systems and engineering structures can reveal many of the system's fundamental features and, therefore, become a basis for the study of inverse problems. In this series of papers, we take a reverse, direct-problem point of view; namely, given the shapes of animals, can we see the patterns of their motions or behaviors through their eigenmode analysis? This modal analysis, we believe, has never been done for living animals. Our modal analysis emphasizes dynamics, which is achieved by visualization through video animation by incorporating the time-harmonic dependence of the eigenmodes. Furthermore, we intend our modal analysis to be more realistic by encompassing the situation of the presence of a floor. Certain physical interpretations of the motion patterns from modal analysis are made. In addition, by visualization, one can see that symmetry plays an important role in motion patterns. One of our main conclusions is that shapes alone can usefully reflect or explain some animal's behavior or motion patterns.

Keywords Animal shapes · Modal analysis · CAD · Horse · Camel · Motion patterns

Mathematics Subject Classification 92-10 · 92C10 · 92D50

1 Introduction

The main objective of this series of papers is to study the modal analysis of a few selected animals by *their shapes*. We will use elastodynamics to model the bodies of

several long-necked animals, compute their eigenmodes of motion, and try to understand their motion patterns.

The study of shapes is one of the central themes in geometry, applied mathematics and engineering design. A case in point is the determination of shape from acoustic or electromagnetic scattering data. When a linear elastic body vibrates, the dynamic change of shapes generates pressure difference of air around the solid, which then propagates with the same frequencies as acoustic waves in the air. We may recall a famous paper: "Can one hear the shape of a drum" by Kac [1]. For a drum modeled as a thin membrane, it satisfies the 2D wave equation and, therefore, the vibrating frequencies squared are proportional to the eigenvalues of the negative Laplacian for the spatial domain, say with the homogeneous Dirichlet condition. For that domain (and the higher dimensional analogues), Kac posed the question whether knowing all of the eigenvalues of the Laplacian can uniquely determine the domain. The answer has been confirmed to be negative [2]. However, for 2D planar convex domains, under some additional conditions, the answer was found to be positive [3]. Such studies have provided considerable stimuli and inspiration to the modern study of *Inverse Problems*, where partial or full knowledge of the so-called *spectral data* of many oscillation, scattering and heat-transfer problems are used as the basis for reconstructing the whole physical or engineering problem under study.

From the viewpoint of inverse or reconstruction problems, the above underlines the importance of eigenvalue/eigenfrequency spectral analysis of problems in applied mathematics, sciences and engineering. Speaking overall, the spectral analysis of linear, and even certain nonlinear operators, is a major field of analysis in the study of PDEs. Much of the existing mathematical literature in this connection deals with PDE models governed by the wave, heat and electromagnetic equations and systems. However, not much has been done if the system is *biological* involving various *living creatures*, especially *animals*. An animal, quoting from *Biology Online* [4], pertains to any of the eukaryotic multicellular organisms that comprise the biological kingdom of Animalia. Animals possess several characteristics that distinguish them from other living matter. Animals are generally *motile*, meaning that they are capable of moving at will. According to various counts, there are about 5 to 10 millions of species of extant animals in the world today. Among the large class of animals, *homo sapiens* is obviously the most important species from our self-centered point of view. Besides homo sapiens, the livestock animals of cows, horses, pigs, sheep, and poultry must rank the next highest in their importance to the lives and civilization of human beings in the sense that they supply meat to sustain our lives and their raising also forms some of the core activities of the agricultural society. Not to be excluded is the class of fish or shellfish from the freshwater or sea. These animals account for the bulk of the non-vegetarian proteins of our food and grocery purchases in much of the world.

In the study of animals and the analysis of their motions and motion patterns, one cannot help but refer to the work of the distinguished Scottish mathematical biologist D'Arcy Wentworth Thompson. He published his pioneering work *On Growth and Form* [5] *in 1917. In this masterpiece, Thompson gave his theory of morphogenesis*, the process by which biological patterns and body structures are formed in animals and plants. During Thompson's era, most biologists were under the great influence of Charles Darwin's work of evolution and, therefore, tended to overemphasize natural

selection and evolution as the fundamental driving forces of the form and structure of living organisms. Consequently, the *roles of physical laws and mechanics* were underemphasized. Thompson advocated *allometry* [6] and hinted at a scientific interpretation of *vitalism* [7]. He has quoted a wealth of examples and finds *correlations between biological shapes and mechanical phenomena.* For example, he pointed out the similarities between the internal supporting structures in the hollow bones of birds and well-known engineering truss structural designs. These issues: allometry, evolution, morphogenesis, vitalism, are all directly or indirectly overlapping with the interest of our work here on shapes, mathematical modeling and motion analysis. D'Arcy Thompson's work in [5], according to today's standards, is mostly descriptive or *qualitative*. But his theory has inspired a generation of young biologists and scientists in advancing morphogenesis to a rigorous *quantitative* level, for example the Alan Turing's famous work [8] on the formation of patterns, such as spots and stripes on leopards and zebras, through nonlinear diffusion. Even so, during Thompson's days, the theories of partial differential equations and continuum mechanics were emerging, computational modeling of (engineering and biological) structures was essentially nonexistent. He was over one hundred years ahead of his time! But now, only during the most recent decade, we have the maturing mathematical and computational modeling software platforms and supercomputers to facilitates research in this direction.

The main methodology in our work is *modal analysis*. The term "modal analysis" likely has originated from structural engineering. It aims at studying dynamic properties of mechanical systems in the *frequency domain*. A vibrating system has *normal modes of vibration, which are the simplest form of vibration with a single-frequency in time.* All the "free vibration" can be decomposed as a linear superposition of such modes. Mathematically speaking, such so-called "modes" are essentially synonymous to *eigenvectors/eigenfunctions* in functional analysis. In this sense, modal analysis can be classified as a subfield of *Fourier analysis.* However, the meaning of modal analysis can take on some more subtlety than this. When an engineer uses the term modal analysis, he/she most likely is referring to some eigensolutions of a finite element approximation of an engineering system. Furthermore, sometimes, for those systems, the boundary conditions (or other constraint conditions), for example, may be rather complex; these may not be described in terms of the "traditional" elegant Dirichlet, Neumann, or Robin types that mathematicians have gotten quite used to. These three types of boundary conditions also tend to have a variational origin. One such example of a non-traditional complex boundary conditions is *contact conditions*. Contact conditions usually are described in terms of local (finite element) node relations at places of contact, where potential penetration of a slave mode through a master segment is to be checked. In this paper, we will need to use contact conditions to model the contacts between an animal with the ground, for example, when an animal is walking or running on the ground. The modeling of contact with the environment is "tricky" as the contact between the feet and the ground is on-and-off depending on the motion of feet. Potentially, one of the animal's feet can get stuck into the ground if the ground support is not strong enough (even though we do not really consider such a situation, but the possibility must be incorporated into the model). Our modal analysis is a *dynamic harmonic motion, where the square of the frequency is the eigenvalue of a certain elastic operator.* Throughout our paper, we will use the the three terms:

modes (of motion), *normal modes and eigenmodes*, in a cavalier way to mean the same thing. There is still one more caveat: eigenmode shapes are highly *model dependent*. As we will see shortly, our computational models are still crude. Necessarily, such modeling errors will generate many "spurious modes" that do not rightfully belong to the biomechanical system that we are trying to model. A "rule of thumb" in assessing whether a computed mode is acceptable or reasonable is that the sequential order of the mode cannot be too large. Usually engineers or modelers would discard computed modes beyond a couple of hundred. Still, for even low-order modes, the modeler must assess and determine their validity, correctness and reasonableness judiciously. As a consequence, modal analysis has brought on a strong "empirical flavor" to this type of methodology that is not *mathematically rigorous*. We readily concede that this is true. However, modal analysis continues to be important because it is *highly useful in applications*.

As we have noted above, there exist millions of species of animals on our planet. It would be nice to be able to study them all at a single stretch in this paper, however, in effect, the sheer volume of work would make it difficult if not impossible. One of the main reasons is that many animals have different shapes, and even similar shapes can have different types of modes of motions. In this series of papers, we are limiting our objects for consideration to have a common *trait of long necks*, such as, in alphabetical order, the camel, dinosaur, duck, giraffe, goose, and horse. In addition to the feature of long necks, the following are reasons for the selection:

(i) A duck and a goose are selected because their body shapes are similar but otherwise the latter has a longer neck so we may compare certain effects of the length of necks;

(ii) A camel and a horse are selected as both are common beasts of burden, and their walking and running gaits are somewhat better understood by the common folk;

(iii) A Tyrannosaurus (T-Rex) dinosaur is selected because dinosaurs' ferocious look attracts attention. It has been extinct for million years, but our study may potentially recover some of their motion patterns and gaits.

(iv) Both T-Rex and giraffe have long necks, however, their body shapes are otherwise rather different, as a T-Rex has a much longer and heavier tail, but shorter legs;

Our aim is to study their fundamental modes of motion in the hope of synthesizing some similarities according to their common shape feature of long necks. Nevertheless, as it turns out, this aim seems to be still quite lofty. Our major findings are limited. What we have found can be summarized in general terms, as follows:

(1) Symmetry plays a highly important role in the shapes and order of occurrences of eigenmodes;

(2) Many computed modes of motion manifest the observable motions of those animals. Therefore, animals' shapes alone do reflect or even determine those animals motion patterns.

(3) Many modes can be associated or interpreted with physiological or social significance.

(4) There also exist many "spurious" modes, due to modeling deficiencies, which are unnatural and must be dismissed.

Our plan for the series of five papers (called Part I, Part II, · · · , Part V) is as follows:

In Part I, we focus our attention on the modes of motion of a horse and a camel, and discuss them in detail. One hundred modes for each animal will be displayed. In Part II, we discuss the Fourier decomposition that provides a self-consistent verification of the modal analysis methodology. In Part III, we study the dinosaur, duck, eagle, giraffe and goose, and make some comparisons. For each animal, one hundred modes will be displayed.. In Part IV, we provide the computational geometric construction methodology, recipe and tutorials. In Part V, we study the animation of a T-Rex motion, by combining artistic rendering with scientific rendering with model refinement, and the interaction of the T-Rex with some simple terrain.

We organize this paper, Part I, as follows: In Sect. 2, we discuss the motivation, and review some past work of relevant interest. In Sect. 2, we compare the lumped parameter approach with our distributed parameter modeling, and introduce modal analysis. Section 3 provides the abstract functional space setting with some basic properties about the rigid-body motion established. Sections 6 and 7 contains the results of modal analysis of a horse, respectively, with or without a floor, where 100 modes are displayed for each case with discussions. Section 7 contains the modal analysis counterpart results for a camel. Section 8 provides a summary of this paper.

2 A Lumped Parameter Model for a Horse, Versus a Distributed Parameter Model

Lumped parameter models, which use ODEs to describe and represent systems under study, have had a long history of development. For example, in the study of human body movement and vibration (cf. [9, 10], for example), researchers have built mechanical analogs for various parts of the human body such as the head, limbs, joints, torso, internal organs, soft tissues, etc., as discrete masses, dampers and springs. A set of coupling parameters are then determined empirically, and a system of ODEs is formed. Such an ODE system can be as small as 3×3 or 4×4 for a human body, or as large as several hundred millions by hundred millions based on atom-by-atom modeling in molecular biology. This approach has been rather standard and, in some respects, can even be useful.
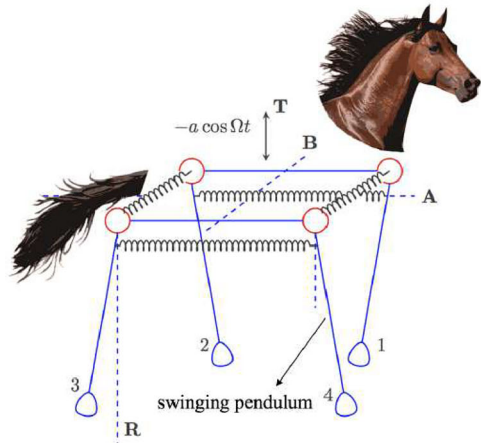
As a main animal subject under study in this paper is the horse, here we mention a nice prior work [11] by van der Weele and Banning. In [11], model of a horse is built as a 4×4 coupled system of nonlinear ODEs as follows (Fig. 1).

The in-phase and out-of-phase motions of any four-legged animal, as depicted in Fig. 2, can be interpreted as representing, respectively, the *pronk, bound, pace and trot motions* of the animal. The use of a coupled pair of simple pendulum to model the back and forth motion of legs is ingenious.

As nice results as the above lumped-parameter modeling may have offered, as with any modeling it has drawbacks, deficiencies and difficulties: The most serious one is the *lack of fidelity*. If we use a lumped mass to represent a horse leg hanging on a pendulum, then even if we can capture certain back-and-forth swing motions of a leg, we will miss out too much of other features of the motion such as knee bending, leg torsion, and lateral side swing. These are true 3D motion features which can only be captured by 3D continuum modeling. That is, we must respect the 3D nature and

$$\ddot{\vartheta}_1 + \gamma\dot{\vartheta}_1 + \frac{1}{l}(g + a\Omega^2 \cos\Omega t)\sin\vartheta_1 + f_B(\vartheta_1, \vartheta_2)$$
$$+ f_A(\vartheta_1, \vartheta_4) = 0,$$
$$\ddot{\vartheta}_2 + \gamma\dot{\vartheta}_2 + \frac{1}{l}(g + a\Omega^2 \cos\Omega t)\sin\vartheta_2 + f_B(\vartheta_2, \vartheta_1)$$
$$+ f_A(\vartheta_2, \vartheta_3) = 0,$$
$$\ddot{\vartheta}_3 + \gamma\dot{\vartheta}_3 + \frac{1}{l}(g + a\Omega^2 \cos\Omega t)\sin\vartheta_3 + f_B(\vartheta_3, \vartheta_4)$$
$$+ f_A(\vartheta_3, \vartheta_2) = 0,$$
$$\ddot{\vartheta}_4 + \gamma\dot{\vartheta}_4 + \frac{1}{l}(g + a\Omega^2 \cos\Omega t)\sin\vartheta_4 + f_B(\vartheta_4, \vartheta_3)$$
$$+ f_A(\vartheta_4, \vartheta_1) = 0.$$

(a)   (b)

Fig. 1 A lumped parameter model according to van der Weele and Bannin [11] for a 4-legged animal. In the figure, A is the left-right exchange, B is the front-hind exchange, R is the reflection of the pendulums, and T is the time translation over one driving period. The head and tail are assumed to be massless. For the choices of the coupling functions f_A and f_B, see [11]. (Adapted from [11, Fig. 14])

(a)   (b)
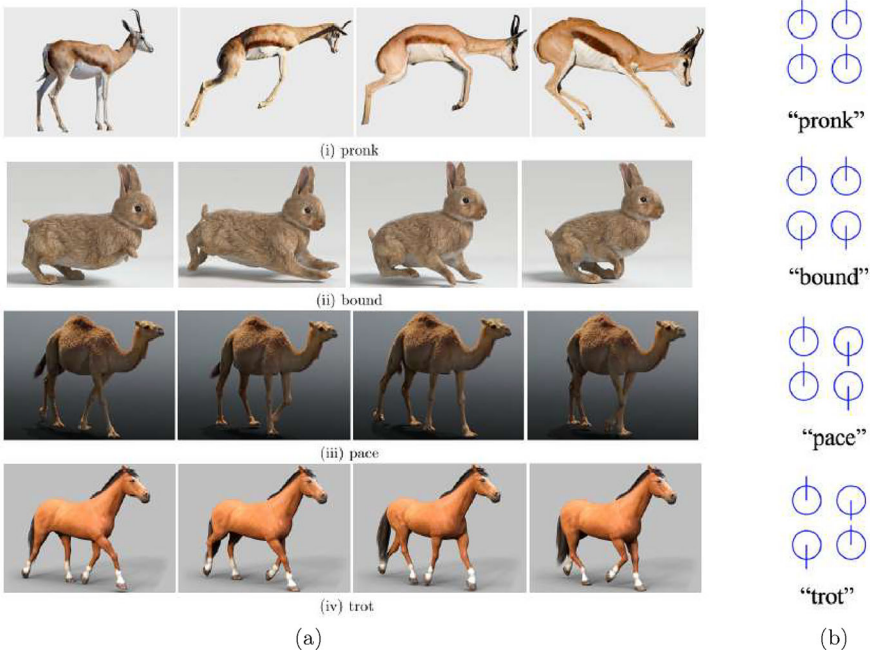
Fig. 2 a The four basic gaits of pronk, bound, pace and trot. **b** The in-phase and out-of-phase motions of the four legs of a 4-legged animal as modeled in Fig. 1. (Graphics adapted from [11, Figs. 15 and 16])

geometry of the object under investigation. There are also many associated problems such as the process of identification of the various coupling parameters in an artificially partitioned system of head, limbs, torso and other parts of the body, which can be highly ad hoc. Using such models to perform simulations, one can easily find that the results are hard to interpret as they are not "the real thing". Elsewhere, in bacteriology and virology, for a microbiological system where, as aforementioned, a model built on the atom-by-atom interactions involving hundreds of millions of coupled mass-spring-dashpot ODEs, it is costly and time-consuming to simulate on a supercomputer. This constitutes another extreme class of lumped-parameter models with too many ODEs.

Banning, van Der Weele and their collaborators have published a series of interesting papers advancing the theories of animal's motion patterns, symmetries, nonlinear couplings, mathematical/physical modeling and bifurcation; see [12–16]. Such work is very much in consonance with D'Arcy Thompson's thinking that physical laws and mechanics should play an important role in the study of "growth and form". Nevertheless, they did not seem to be aware of Thompson's work as [5] was never cited in [11–16].

A much more preferable, faithful way of modeling is a *distributed parameter approach* by treating the animal bodies as a *continuum*, and employ continuum mechanics. This will lead to a PDE model. This approach has already been introduced in an earlier paper [17] where several coauthors there overlap also as the coauthors here. To make this paper sufficiently self-contained, in what follows, we will give it a succinct description.

In our modeling of the various kinds of animals in this series of papers, we make the simplifying assumption that these animals form a uniform, homogeneous solid mass. They take the shapes and scales as closely as the "real animals per se" as possible. We wish to perform modal analysis by computing their modes of vibration. The animals' vertebrates, bones, joints, tendons, internal organs, body fluids, etc., are *not modeled*. Therefore, the computed modes in our work are *determined by shapes alone*. The simplifying assumptions have obviously constituted some over-simplification. However, as our work will show, *animals' shapes alone can determine many of their motion patterns.*

We are now in a position to describe modal analysis based on continuum mechanics. For a solid continuum occupying Ω in 3D, Newton's law of motion dictates that

$$\rho \frac{\partial^2 \mathbf{u}}{\partial t^2} = \nabla \cdot \boldsymbol{\sigma} + \mathbf{f}, \quad \text{at } (x, y, z) \in \Omega, \text{ at time } t. \tag{2.1}$$

Here, ρ is the density of mass, $\mathbf{u} = \mathbf{u}(x, y, z, t)$ is the displacement vector, $\boldsymbol{\sigma} = \boldsymbol{\sigma}(x, y, z, t)$ is the stress tensor, and $\mathbf{f} = \mathbf{f}(x, y, z, t)$ is the body force per unit volume. The equation above says that, at point (x,y,z) at time t, on the LHS of (2.1), the inertial force per unit volume is the sum, on the RHS, of the contact force plus body force, per unit volume. The contact force is in effect only when particles get into contact with each other, while the body force can act across distance (without getting into contact) such as the gravitational and/or electromagnetic forces.

The boundary conditions are

$$\mathbf{u} = \tilde{\mathbf{u}} \text{ on } \partial\Omega \text{ at time } t, \qquad \text{(Dirichlet boundary condition)}$$
$$\boldsymbol{\sigma} \cdot \mathbf{n} = \tilde{\mathbf{c}} \text{ on } \partial\Omega \text{ at time } t, \qquad \text{(Neumann boundary condition)}$$

The usual linear strain tensor on $\Omega(t)$ is

$$\boldsymbol{\varepsilon} = \boldsymbol{\varepsilon}(\mathbf{u}) = \frac{1}{2}\left[\nabla\mathbf{u} + (\nabla\mathbf{u})^\top\right], \quad \boldsymbol{\varepsilon} = \boldsymbol{\varepsilon}(x, y, z, t), \quad (x, y, z) \in \Omega. \qquad (2.2)$$

The above has a decomposition into an elastic part $\boldsymbol{\varepsilon}^e$ and a plastic part $\boldsymbol{\varepsilon}^p$:

$$\boldsymbol{\varepsilon} = \boldsymbol{\varepsilon}^e + \boldsymbol{\varepsilon}^p. \qquad (2.3)$$

Assume the constitutive relation

$$\boldsymbol{\sigma} = \mathbf{C}\boldsymbol{\varepsilon}^e. \qquad (2.4)$$

For an isotropic, homogeneous, elastic solid, we have $\boldsymbol{\varepsilon}^p \equiv 0$, and the following holds:

$$\sigma_{ij} = \lambda\left(\sum_{k=1}^{3} \frac{\partial\mathbf{u}_k}{\partial\mathbf{x}_k}\right)\delta_{ij} + 2\mu\varepsilon_{ij}, 1 \geq i, j \leq 3. \qquad (2.5)$$

One can derive from (2.1)–(2.5) the linear elastodynamic equations of motion

$$\rho\frac{\partial^2\mathbf{u}}{\partial t^2} = (\lambda + \mu)\nabla(\nabla \cdot \mathbf{u}) + \mu\nabla^2\mathbf{u} + \mathbf{f} \quad \text{on } \Omega(t). \qquad (2.6)$$

Here, the force $\mathbf{f}$ is gravity per unit volume. The coefficients λ and μ are the usual Lamé constants for the material.

Finite element discretization

$$\mathbf{u} \approx \mathbf{u}_{(h)} = \sum_{k=1}^{n_h} \alpha_k^{(h)}(t)\phi_k^{(h)}(x, y, z) \qquad (2.7)$$

provides approximation to the displacement $\mathbf{u}$ with mesh size h, which, after a Ritz–Galerkin procedure [18], yields a finite-dimensional ordinary differential equation in the form

$$\mathbf{M}\ddot{\mathbf{u}}(t) + \mathbf{C}\dot{\mathbf{u}}(t) + \mathbf{K}\mathbf{u}(t) = \mathbf{P}(t), \qquad (2.8)$$

where $\mathbf{u}(t) = (\alpha_1^{(h)}(t), \alpha_2^{(h)}(t), \dots, \alpha_{n_h}^{(h)}(t))$, with initial conditions

$$\mathbf{u}(0) = \mathbf{u}_0 \in \mathbb{R}^{n_h}, \dot{\mathbf{u}}(0) = \mathbf{u}_1 \in \mathbb{R}^{n_h}, \qquad (2.9)$$

where $\mathbf{u}_0$ and $\mathbf{u}_1$ are uniquely determined from the initial conditions

$$\mathbf{u}(x, y, z, 0) = \mathbf{u}_0(x, y, z), \quad \frac{\partial}{\partial t}\mathbf{u}(x, y, z, 0) = \mathbf{u}_1(x, y, z) \qquad (2.10)$$

In the linear case ($\epsilon^P \equiv 0$) the superposition principle gives

$$\mathbf{u}(t) = \mathbf{u}_p(t) + \sum_{j=1}^{n_h} c_j \mathbf{w}_j(t), \quad c_j \in \mathbb{C} \text{ (field of complex numbers)}, \tag{2.11}$$

where $\mathbf{u}_p(t)$ is a particular solution related to forced vibration, while $\mathbf{w}_j(t)$ satisfies the homogeneous equation system

$$\mathbf{M}\ddot{\mathbf{w}}_j(t) + \mathbf{C}\dot{\mathbf{w}}_j(t) + \mathbf{K}\mathbf{w}_j(t) = 0, \quad j = 1, 2, \ldots, n_h. \tag{2.12}$$

Set $\mathbf{w}_j(t) = e^{\lambda_j t} \boldsymbol{\phi}_j$,

$$(\lambda_j^2 \mathbf{M} + \lambda_j \mathbf{C} + \mathbf{K})\boldsymbol{\phi}_j = \mathbf{O} \in \mathbb{R}^{n_h}. \tag{2.13}$$

Note that λ_j is a root to the algebraic equation

$$\det\left(\lambda^2 \mathbf{M} + \lambda \mathbf{C} + \mathbf{K}\right) \equiv p(\lambda) = 0. \tag{2.14}$$

For the case of *harmonic motions* without damping, the term C is dropped to give

$$\mathbf{M}\ddot{\mathbf{w}}_j(t) + \mathbf{K}\mathbf{w}_j(t) = 0, \quad j = 1, 2, \ldots, n_h. \tag{2.15}$$

We obtain solutions $\mathbf{w}_j(t)$,

$$\mathbf{w}_j(t) = e^{i\omega_j t} \boldsymbol{\phi}_j, \text{ (vibrating mode)} \tag{2.16}$$

where ω_j satisfies

$$(-\omega_j^2 \mathbf{M} + \mathbf{K})\boldsymbol{\phi}_j = 0. \tag{2.17}$$

At this point, we can solve the eigenvalue problem (2.17) with LS-DYNA for the frequencies ω_j, eigenvalues ω_j^2, and the corresponding eigenvectors (mode shapes) $\boldsymbol{\phi}_j$. The Block Shift and Invert Lanczos eigensolver is used in LS-DYNA to compute the normal modes and mode shapes for (2.17). For more details about the Lanczos algorithm, refer to [19, pp. 799–800, Section 40]. In our calculations, we have also used LS-DYNA software to check the *stability and convergence* properties of our computational processes.

Computationally, the above modal analysis can be performed by LS-DYNA Software using the following keywords:

*CONTROL_MPLICIT_EIGENVALUE
*CONTROL_MPLICIT_GENERAL
*CONTROL_MPLICIT_SOLUTION

Here, we note some differences between eigenfunction analysis and modal analysis: (1) Usually, eigenfunctions refer to eigensolutions of a system of PDEs in the form

$$A\phi(x) = \lambda\phi(x), \quad \phi \in H, \ H : \text{a Hilbert space},$$

where boundary conditions have already been incorporated into the functional Hilbert space H, while numerical eigenfunction analysis refers to a *discretized form* of above in terms of matrices:

$$A_h \phi_h = \lambda_h \phi_h, \phi_h \in V_h, \ V_h \text{ is an approximation finite element space,}$$
$$h = \text{size of the discretization parameter.}$$

Such a discretization is usually obtained through some form of calculus of variations.

(2) However, modal analysis can accommodate more *flexibility* as it is expressed in terms of matrices and nodes of finite elements, which can or may not be obtainable through ordinary calculus of variations. A practical example is the inclusion of *contact boundary conditions*.

Note that if the solid is nonlinear, then usually there will also be associated super- and sub-harmonics accompanying the primary frequency of vibration. Thus, one may very well need to solve a nonlinear eigenvalue problem instead.

Here are our remaining comments regarding challenges of modal analysis:

(1) Grid generation and discretization:
   Multi-scales: feathers, tails, body-parts in contact
   Multi-phases: body fluids
   Internal organs, musculature, soft and connective tissues, fibers
(2) Skeletal structures and joints (so far lacking, as well as the items in (1) above).
(3) Lower dimensional structures: e.g., the webbed feet of ducks and geese.
(4) Interactions with the environment: contact with terrain and the presence of obstacles.
(5) Large deformation: stretched-out wings and their flapping.
(6) Software and supercomputing cost.

3 The Functional Space Formulation on the Elastodynamic Equation and Its Null Space

Return to the elastodynamic equation (2.6). We can write it in a first order form

$$\frac{\partial}{\partial t} \begin{bmatrix} \mathbf{u} \\ \rho \frac{\partial u}{\partial t} \end{bmatrix} = \begin{bmatrix} 0 & \frac{1}{\rho} \\ (\lambda + \mu)\nabla \cdot (\nabla) + \nabla^2 & 0 \end{bmatrix} \begin{bmatrix} \mathbf{u} \\ \rho \frac{\partial u}{\partial t} \end{bmatrix} + \begin{bmatrix} 0 \\ \mathbf{f} \end{bmatrix}, \tag{3.1}$$

with corresponding energy functional $E(t)$ defined by

$$E(t) = \int_\Omega \left[\frac{1}{2}\rho \left|\frac{\partial u}{\partial t}\right|^2 + \frac{1}{2} \sum_{i,j=1}^n \sigma_{ij} \cdot \varepsilon_{ij} \right] dx \tag{3.2}$$

$$= \frac{1}{2} \int_\Omega \left[\rho \left|\frac{\partial u}{\partial t}\right|^2 + \lambda|\nabla \cdot u|^2 + \sum_{i,j=1}^3 \mu \left(\frac{\partial u_i}{\partial x_j} + \frac{\partial u_j}{\partial x_i}\right)^2 \right] dx. \tag{3.3}$$

Let $H^k(\Omega)$ denote the usual Sobolev space of order k. The underlying semi-normed space for (3.3) is

$$\begin{bmatrix} u \\ v \end{bmatrix} \in \left[H^1(\Omega) \right]^3 \times \left[L^2(\Omega) \right]^2,$$

with semipositive definite energy inner product defined by

$$\left\langle \begin{bmatrix} u_1 \\ v_1 \end{bmatrix}, \begin{bmatrix} u_2 \\ v_2 \end{bmatrix} \right\rangle_E = \int \left[\rho v_1 v_2 + \lambda \left(\nabla u_1 \cdot \nabla u_2 \right) \right.$$
$$\left. + \sum_{i,j=1}^{3} \mu \left(\frac{\partial u_{1i}}{\partial x_j} + \frac{\partial u_{2j}}{\partial x_i} \right) \left(\frac{\partial u_{2i}}{\partial x_j} + \frac{\partial u_{1j}}{\partial x_i} \right) \right] dx \qquad (3.4)$$

This pairing (3.4), in general, will only be semipositive definite. But if u in (2.5) satisfies the fixed boundary condition $\mathbf{u}|_{\partial\Omega} = 0 \in \mathbb{R}^3$, for all $t \geq 0$, then $\langle \, , \, \rangle_E$ becomes a positive definite inner product on $\left[H_0^1(\Omega) \right]^3 \times \left[L^2(\Omega) \right]^3$, due to the first Korn's inequality [20],

$$\sum_{i,j=1}^{3} \int_\Omega \varepsilon_{ij}^2 dx = \frac{1}{4} \sum_{i,j=1}^{3} \int_\Omega \left(\frac{\partial u_i}{\partial x_j} + \frac{\partial u_i}{\partial x_i} \right)^2 dx \geq C \|u\|_{H^1(\Omega)]^3}^2,$$

for some $C > 0$, for all $\mathbf{u} \in \left[H_0^1(\Omega) \right]^3$.

For later use, here we also mention the second Korn's inequality:
"There exists $C > 0$ such that

$$\sum_{i,j=1}^{3} \int_\Omega \varepsilon_{ij}^2 dx = \frac{1}{4} \sum_{i,j=1}^{3} \int_\Omega \left(\frac{\partial u_i}{\partial x_j} + \frac{\partial u_j}{\partial x_i} \right)^2 dx \geq C \|u\|_{[H^1(\Omega)]^3}^2,$$

for all $\mathbf{u} \in \widetilde{H}(\Omega) \subseteq \left[H^1(\Omega) \right]^3$, where

$$\widetilde{H}(\Omega) \stackrel{\text{def.}}{=} \left\{ \mathbf{u} \in \left[H^1(\Omega) \right]^3 \mid \mathbf{u} \perp (\mathbf{Bx} + \mathbf{b}), \right.$$

$$\left. \text{for all skew-symmetric } 3 \times 3 \text{ matrix } \mathbf{B} \text{ and constant } \mathbf{b} \in \mathbb{R}^3 \right\}. \text{"} \qquad (3.5)$$

In the above, $\mathbf{u} \perp (\mathbf{Bx} + \mathbf{b})$, and the orthogonality "$\perp$" refers to the standard inner-product of $\left[L^2(\Omega) \right]^3$.

We may note that the subspace

$$\{\mathbf{v} \in [H^1(\Omega)]^3 \mid \mathbf{v} = \mathbf{Bx} + \mathbf{b}, \mathbf{B} \text{ is skew-symmetric}, \mathbf{b} \in \mathbb{R}^3\}$$

has 9 degrees of freedom. For an elastodynamic continuum subject to the force-free boundary condition, there will be *six modes* corresponding to *rigid body motions*.

These rigid body motions do not undergo any elastic deformation on the whole body of the continuum and, therefore, the corresponding frequency is *zero*. These six modes correspond to the *six degrees of freedom of motion*, namely, three are translations along the three coordinate axes, while the other three correspond to the *rotations of pitch, roll and yaw*. Here, we sometimes call them *the trivial modes*.

The above seems to be a known fact among the experts in the theory of elasticity, but we have not yet seen any statements in the literature. We have discovered them only after our work on modal computations. In the following, we state it as a theorem.

Theorem 3.1 *Let Ω be a bound domain in $\mathbb{R}^3$ with sufficiently smooth boundary $\partial\Omega$. Then, the boundary value problem*

$$\begin{cases} (\lambda + \mu)\nabla(\nabla \cdot \mathbf{u}) + \mu\nabla^2\mathbf{u} = 0 & on\ \Omega, \\ \displaystyle\sum_{j=1}^{3} \sigma_{ij}n_j = 0\ on\ \partial\Omega, & for\ i = 1, 2, 3 \end{cases} \tag{3.6}$$

has a six dimensional null space spanned by

$$\left\{ \begin{bmatrix} 0 \\ -x_3 \\ x_2 \end{bmatrix}, \begin{bmatrix} x_3 \\ 0 \\ -x_1 \end{bmatrix}, \begin{bmatrix} -x_2 \\ x_1 \\ 0 \end{bmatrix} \right\} \cup \left\{ \begin{bmatrix} 1 \\ 0 \\ 0 \end{bmatrix}, \begin{bmatrix} 0 \\ 1 \\ 0 \end{bmatrix}, \begin{bmatrix} 0 \\ 0 \\ 1 \end{bmatrix} \right\}. \tag{3.7}$$

Proof From (3.6), using integration by parts, we have

$$0 = \int_{\Omega} \left[(\lambda + \mu)\nabla\left(\nabla \cdot \mathbf{u} + \mu\nabla^2\mathbf{u}\right) \right] \cdot \mathbf{u} dx$$

$$= -\int_{\Omega} \left[(\lambda + \mu)|\nabla \cdot \mathbf{u}|^2 + \sum_{i,j=1}^{3} 2\mu \left(\frac{\partial u_i}{\partial x_j} + \frac{\partial u_j}{\partial x_i} \right)^2 \right] dx + \sum_{i,j=1}^{3} \int_{\partial\Omega} \sigma_{ij} n_j u_i d\sigma$$

$$= -\int_{\Omega} \left[(\lambda + \mu)|\nabla \cdot \mathbf{u}|^2 + \sum_{i,j=1}^{3} 2\mu \left(\frac{\partial u_i}{\partial x_j} + \frac{\partial u_j}{\partial x_i} \right)^2 \right] dx$$

$$\leq -\frac{1}{C} \|\mathbf{u}\|_{[H^1(\Omega)]^3}^2 \tag{3.8}$$

according to Korn's inequality, as stated in (3.5), if $\mathbf{u} \in \tilde{H}(\Omega)$, for some $C > 0$ independent of $\mathbf{u}$.

For (3.8) to hold, we must have

$$\begin{cases} \text{either}\quad \mathbf{u} \equiv 0\quad \text{on}\quad \partial\Omega, & (3.9) \\ \text{or}\quad \mathbf{u} = \mathbf{B}x + \mathbf{b},\ \text{for some skew-symmetric}\ 3 \times 3\ \text{matrix}\ \mathbf{B}\ \text{and}\quad \mathbf{b} \in \mathbb{R}^3. & \\ & (3.10) \end{cases}$$

If (3.9) holds, $\mathbf{u}$ satisfies both $\mathbf{u}|\partial\Omega = 0$ and $\sum_{j=1}^{3} \sigma_{ij} n_j = 0$ on $\partial\Omega = 0$ for $i = 1, 2, 3$. Thus $\mathbf{u}$ is overdetermined. A little more arguments similar to case (3.10) shows that $\mathbf{u}$ is a trivial solution which is uninteresting. So we only need to consider (3.10). The set

$$\left\{ v : \Omega \to \mathbb{R}^3 \mid v = \mathbf{B}x, \mathbf{B} \text{ is an arbitrary } 3 \times 3 \text{ skew-symmetric matrix} \right\}$$

is a 3-dimensional subspace of $\left[H^1(\Omega) \right]^3$. If $\mathbf{u} = \mathbf{B}x$ for a skew-symmetric $\mathbf{B}$ and

$$\sum_{i,j=1}^{3} \sigma_{ij} n_j = 0, i = 1, 2, 3, \text{ on } \partial\Omega,$$

then because such (n_1, n_2, n_3) spans $\mathbb{R}^3$ and $\left[\sigma_{ij} \right]$ is a constant 3×3 matrix, we must have

$$\sigma_{ij} = \lambda \left(\sum_{k=1}^{3} \frac{\partial \mathbf{u}_k}{\partial \mathbf{x}_k} \right) \delta_{ij} + 2\mu \left(\frac{\partial \mathbf{u}_i}{\partial \mathbf{x}_j} + \frac{\partial \mathbf{u}_j}{\partial \mathbf{x}_i} \right) = 0, \ 1 \le i, j \le 3.$$

The above, together with $\mathbf{u} = \mathbf{B}x$ for a skew-symmetric $\mathbf{B}$, after straightforward calculations, gives us the 3-dimensional subspace spanned by the first three states as listed in (3.7), plus the 3-dimensional space of constant vectors.

The rest of the proof is obvious.   □

Remark 1 Among the first three states as listed in (3.7),

$$\left\{ \begin{bmatrix} 0 \\ -x_3 \\ x_2 \end{bmatrix}, \begin{bmatrix} x_3 \\ 0 \\ -x_1 \end{bmatrix}, \begin{bmatrix} -x_2 \\ x_1 \\ 0 \end{bmatrix} \right\},$$

they represent rotations as they are, respectively, equal to

$$\begin{bmatrix} 0 \\ -x_3 \\ x_2 \end{bmatrix} = \begin{bmatrix} 1 \\ 0 \\ 0 \end{bmatrix} \times \mathbf{x}, \begin{bmatrix} x_3 \\ 0 \\ -x_1 \end{bmatrix} = \begin{bmatrix} 0 \\ 1 \\ 0 \end{bmatrix} \times \mathbf{x}, \begin{bmatrix} -x_2 \\ x_1 \\ 0 \end{bmatrix} = \begin{bmatrix} 0 \\ 0 \\ 1 \end{bmatrix} \times \mathbf{x}.$$

Their curls are pointing, respectively, to the directions of $\vec{i}$, $\vec{j}$ and $\vec{k}$ with magnitude 2.

These three states will manifest themselves in our later calculations as rotations, while the last three constant states in (3.7) represent translations.

4 The CAD Horse Model

The horse is intended to be a thoroughbred [21]. Thoroughbreds have a lean body and long legs, which have become exemplar of a racehorse and stud horse in America; see

Fig. 3 Photo of a thoroughbred, selected from [21]

Fig. 3. In our work to ensue, we have gone through several rounds of design iterations to try to capture these important features.

The CAD horse model in our modal analysis was initially based on the designs from *Blender* [22]. It is a low-polygon count STL (an acronym that stands for *stereolithography*,—a popular 3D printing technology) file meant mainly for 3D printing and does not have easily adjustable appendages. See Fig. 3. Here, by "low polygonal count" we mean that the number of vertices, edges and faces in the polygonal mesh counts in the order of 10,000. The horse from *Blender* has a short and pointed tail which does not accurately reflect the tail of a horse. By extending the length of the tail and also adding in some minor details such as a small upward curving from the base of the tail, we feel that the visual effects of our simulation has been somehow enhanced. A CAD model is yielded as in Fig. 4.

To perform modal analysis, finite element meshes need to be generated from certain transformation of the STL file. Depending on the geometry of the model, the generated mesh may have holes or gaps or may not even be successfully generated. To avoid such pitfalls, we have used two different CAD packages for testing: SolidWorks [23] and ANSYS Geometry [24] to check the mesh for any failure points such as disconnected or open elements that may occur during our simulation and fix any holes within the geometry to ensure proper mesh generation. More on such geometrical and mesh construction can be found in Part IV of this series of papers (Fig. 5).

In our subsequent finite element calculations, we have used the following parameters and data:

Solid Element Properties Element formulation option: S/R quadratic tetrahedron element with nodal rotations
LS-DYNA revision R12.1-190-gadfcdf9018
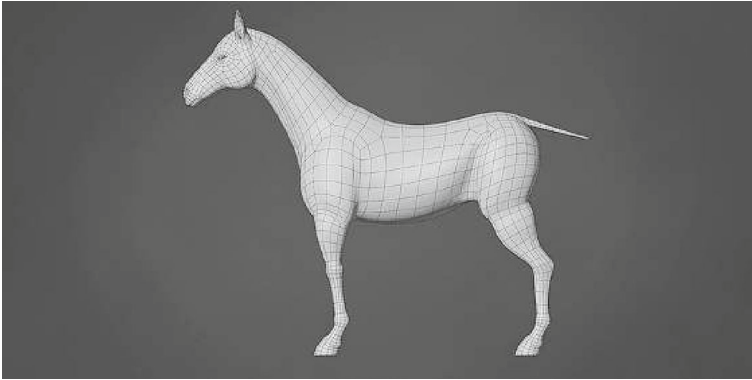
Fig. 4 A CAD model of horse from *Blender* [25]. A shortcoming here is that the tail is too short
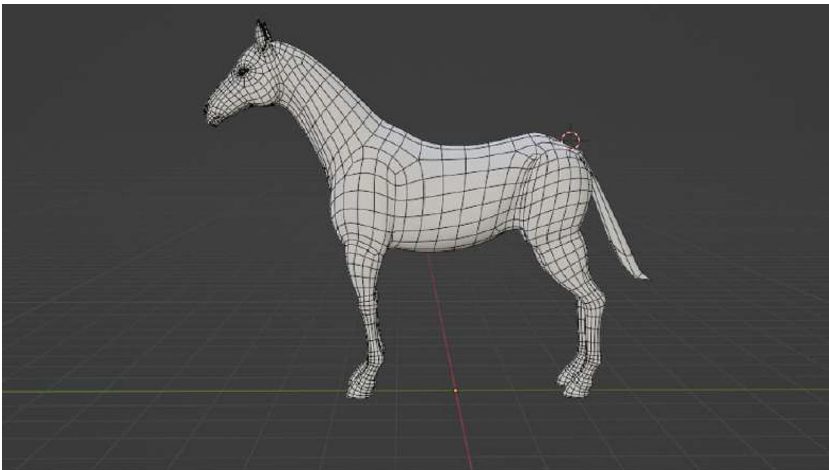
Fig. 5 A refined CAD model obtained by us for the subsequent modal analysis

Number of solid elements	729,102
Number of nodes	129,537
Volume	0.444819 m^3
Area	5.34923 m^2
Height	2.09533 m
Length	2.50984 m
Width	0.600 m
Mass	444.82002 kg

5 Modes of Motion of a Horse

We can now proceed to examine the mode shapes of a thoroughbred horse. As a continuum, there is an infinite number of modes an elastodynamic body can have. If desired, the supercomputer can spew out as many modes of motion as we desire by

Precision	Double
Initial time step for implicit solution	1.0 ms
Material properties	
Density	1000 kg/m^3
Young's modulus	7 GPa
Poisson ratio	0.35
Yield stress	0.47 GPa
Tangent modulus	0.7
Hardening parameter	0.11

refining the mesh of continuum indefinitely. But this would be a futile undertaking as we have pointed out earlier that in the computation process, modeling deficiencies soon creep in and render the computed mode shapes unphysical and meaningless. Only the first few lower order modes will be significant. Partly to demonstrate this point, here we choose the first 30 modes of the horse, and attempt to assign, and attempt to assign relevant physical or biological interpretations. As can be seen from the video collection in (5.1), when the mode number gets higher, many modes can be assessed to be unphysical. See, for example, those shown in Figs. 36, 37 and 38.

Consider the horse with free (Neumann type) boundary condition all over. This means that the horse is *suspending in air*. We first display the lowest order 100 modes in sequential order in the following video:

https://drive.google.com/file/d/1OowZcapc8d0pJ3f9jCYJ7v-YJrX704C3/view?usp =share_link   (5.1)

In the collective video above, the video of each mode contains the legend of scale/magnitude on the right side of the panel, with the Mode # and frequency given on the upper left corner of that panel. Nevertheless, for the rest of the graphics and videos (other than the collective videos), no scale/magnitude legends are given in order to simplify the graphics.

For each mode, one can read from the upper left corner of the video about the frequency of periodic motion, this is ω_j in (2.16) in the unit of kilo-Hertz (kHz). Therein, the magnitude of the motion is also indicated in the color legend on the right of each mode. An assembled table of the frequencies is available in Table 2 in the Appendix.

Fig. 6 This is Mode 1 in (5.1) showing a planar translational displacement type rigid body motion. For video animation, please click https://drive.google.com/file/d/1wkwCLf44p7rrZrxhzJ3rdx2RvXN4SCKH/view?usp=sharing
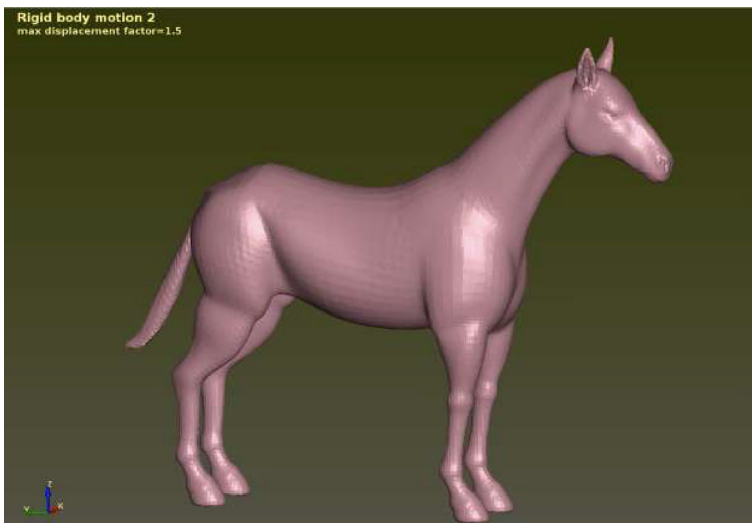
Fig. 7 This is Mode 2 in (5.1) showing a planar translational displacement type rigid body motion. (However, the direction of translation is different from that in Fig. 7). For video animation, please click https://drive.google.com/file/d/1LCOKwJmO9ml4GN6hLs1WdKFXpOgvcs9T/view?usp=sharing

5.1 Six Rigid-Body Motions in the Null Space

We have already noted in Section 4 that there are six (trivial) rigid body modes. They correspond to eigenvalue zero (and zero frequency). We first show these six in Figs. 6, 7, 8, 9, 10, and 11.

Fig. 8 This is Mode 3 in (5.1) showing a vertical translational displacement type rigid body motion. For video animation, please click https://drive.google.com/file/d/1t1S8Kq1DKpo3z5WIQhiRnRYSCyor3mZ9/view?usp=sharing

Fig. 9 This is Mode 4 in (5.1) showing a yaw rotational rigid body motion. For video animation, please see https://drive.google.com/file/d/1AbjigtzwFUhsGNsslDslpBpG9wDjEnXL/view?usp=sharing

5.2 Prominent Low-Frequency Modes and Their Interpretations

Here, we display mode numbers between 7 and 30 in (5.1). They are mostly of a "local nature" and represent some prominent motions of a horse related to gaits and communications. In each graphics, we also give our interpretations to such a motion

Fig. 10 This is Mode 5 in (5.1) showing a pitch rotational rigid body motion. For video animation, please see https://drive.google.com/file/d/1siy5GzXLfUC1mCpyVIzLr-c01jYlCivs/view?usp=sharing

Fig. 11 This is Mode 6 in (5.1) showing a roll rotational rigid body motion. For video animation, please see https://drive.google.com/file/d/1hQ2XH-426HYKtBDRnB6Jfu0U5sF9nMD_/view?usp=share_link

(Figs. 12, 13, 14, 15, 16, 17, 18, 19, 20, 21, 22, 23, 24, 25, 26, 27, 28, 29, 30, 31, 32, 33, 34, 35).

Based on the above graphics and videos, one can continue to peruse the other modes and their motion shapes and find the probable associated biomechanical interpretations (Figs. 36, 37 and 38).
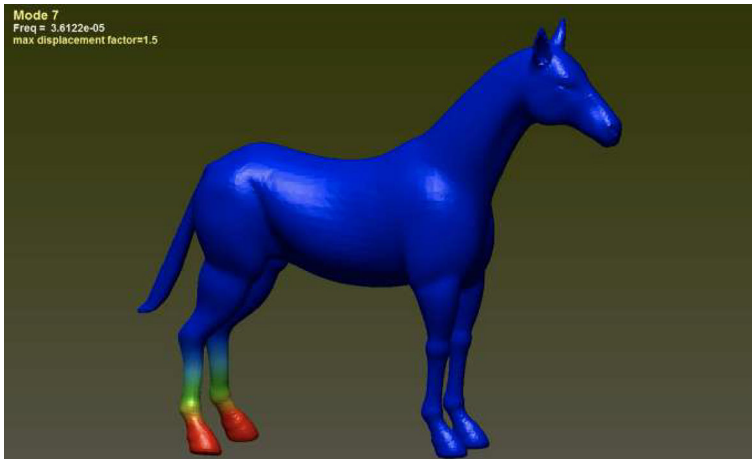
Fig. 12 This is Mode 7, the first non-rigid-body-motion of horse, showing the horse's hind legs lateral motion in-and-out. For video animation, please click https://drive.google.com/file/d/1_EO3_yJUAtHjs2TLe6tu7COrVMJM23dX/view?usp=share_link
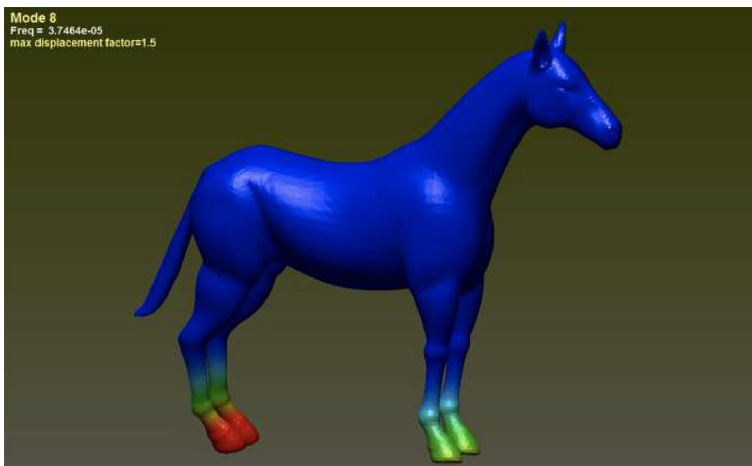
Fig. 13 This is Mode 8, showing the pairwise lateral motion of the fore legs and the hind legs in an out-of-phase way but coordinated rhythm. For video animation, please click https://drive.google.com/file/d/1G6wLEtq_2zq2z4hUpFjDgVlmqWSax2iR/view?usp=sharing

Remark 2 We provide a brief summary of the significance of the Modes 7–30 presented above:

(1) The tail wagging modes are related to horse communications among horses or between a horse and its master.
(2) Modes 13 and 15 are related to the walking or pacing modes of a horse.
(3) Modes 14 and 16 are related to the cantering or galloping motions of a horse;
(4) The sideway motion modes 3, 4, 7, 8, 9, 10, 12, 17, 19, 20, 21, 22, 23, 24, 25, 26, 30 are related to the turning (i.e., changing the directions of movements) motion
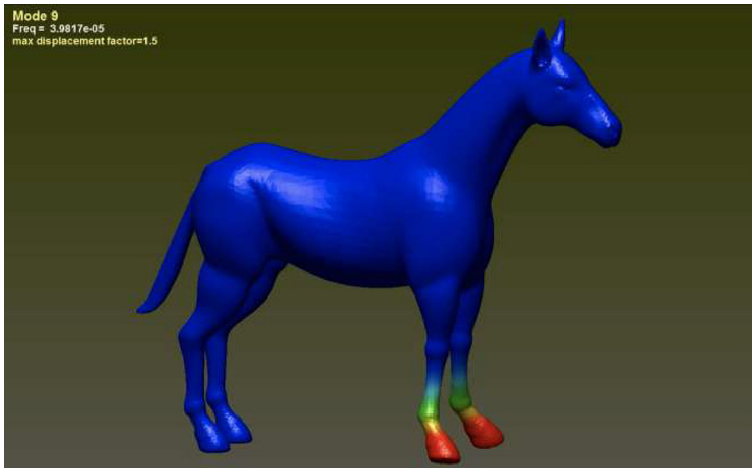
Fig. 14 This is Mode 9, similar to Mode 7 showing a lateral in-and-out motion of the fore legs in contrast to that of the hind legs of Mode 7. For video animation, please click https://drive.google.com/file/d/1lY8fn8ihWTNITV1Ypc5zs9BSYpxR84a2/view?usp=sharing
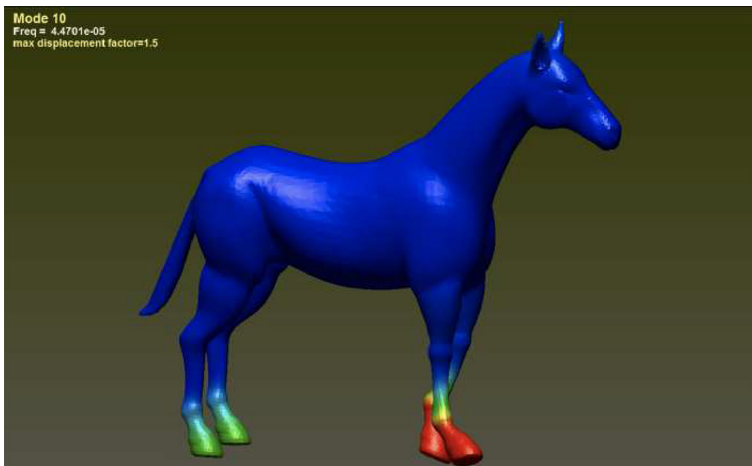
Fig. 15 This is Mode 10, showing an out-of-phase fore legs walking/pacing motion, back-and-forth (or forward-and-backward). There is also some minor motion of the hind legs. For video animation, please click https://drive.google.com/file/d/1l9YKY6tmMcijvZGP3OOBJS2yzGJAGoVG/view?usp=sharing

of a horse. They could also be related to the "injury modes" if the horse cannot withstand the forces or momenta in these motions.

5.3 Some High Frequency Spurious Modes

When the mode number gets high, we can begin to see elastic deformations that are odd, strange, unrealistic or grotesque. More and more so when the mode number gets higher.
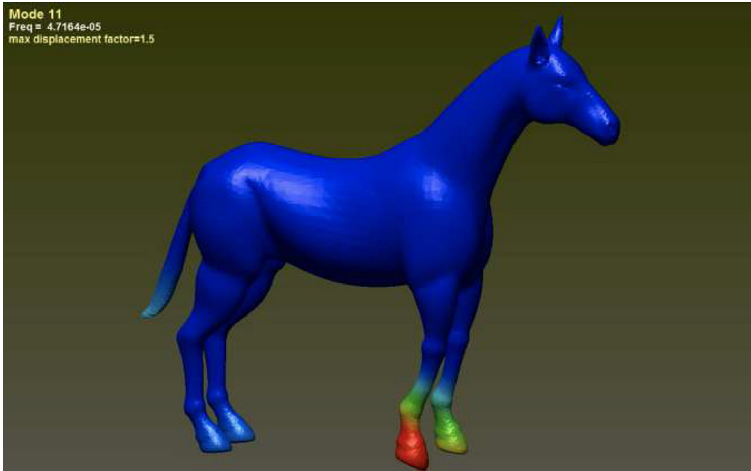
Fig. 16 This is Mode 11, showing an in-phase synchronous fore legs running motion. There is also some minor motion of the hind legs. For video animation, please click https://drive.google.com/file/d/1e-6Z6S3l8pyjoYSjDfErQuowow7Mb4ZJ/view?usp=share_link
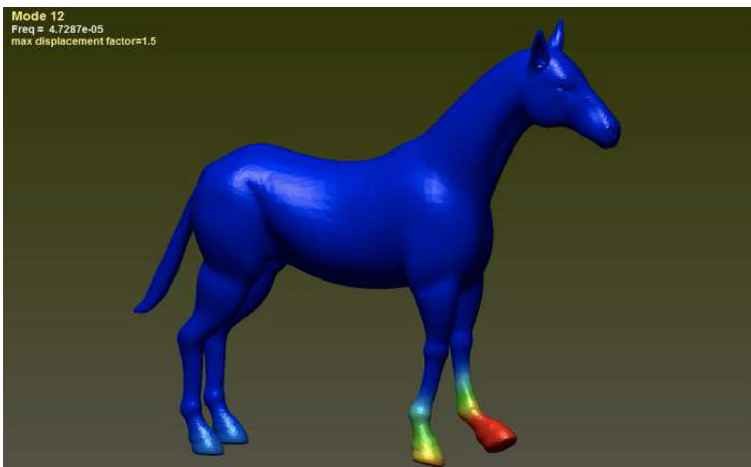
Fig. 17 This is Mode 12, showing an out-of-phase walking/pacing motion of the fore legs. There is also some minor motion of the hind legs. For video animation, please click https://drive.google.com/file/d/1fZ2KJPbKZeN4KpkTHc8Hg1xQ4AR5Tcdg/view?usp=sharing

Here are a few examples. These modes have unnatural, exaggerated appearances and could be related to "injury modes".

5.4 Local Motions of Special Parts of the Horse

In browsing over the set of the 100 modes of the horse, we notice that a majority of the modes involve *only local motions*, for example, those of the feet and legs. In
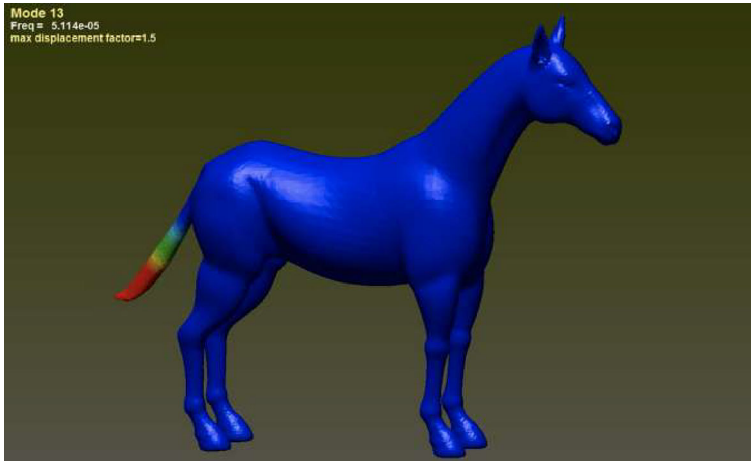
Fig. 18 This is Mode 13, showing up-and-down wagging of the horse's tail. We interpret it as an economic way for a horse to communicate its mood to the master or to other horses. For video animation, please click https://drive.google.com/file/d/1cVWRXIX5VN3Uu98wr4SNg_mmT9H-qNGI/view?usp=sharing
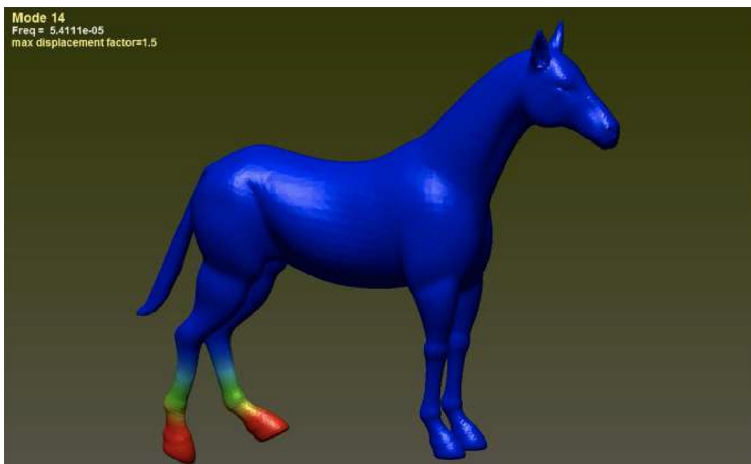
Fig. 19 This is Mode 14, showing an out-of-phase forward-and-backward walking/pacing motion of the hind legs. (There is no motion of the fore legs.) For video animation, please click https://drive.google.com/file/d/1ry6bT30e4YeIc6PCUGvmPpkCeGPUPRdF/view?usp=sharing

addition to the local motions of the feet and legs, there are also many local motions of, respectively, the ears, head, and tail, which have little relation to the motion of the torso or other parts of the horse. Here, we display some of such motions for ears, head and tail, in the following three panels. One can actually see some symmetry at work.

5.4.1 Local Motions of the Horse Ears

We select the local motions of the ears alone and show them in Fig. 39.
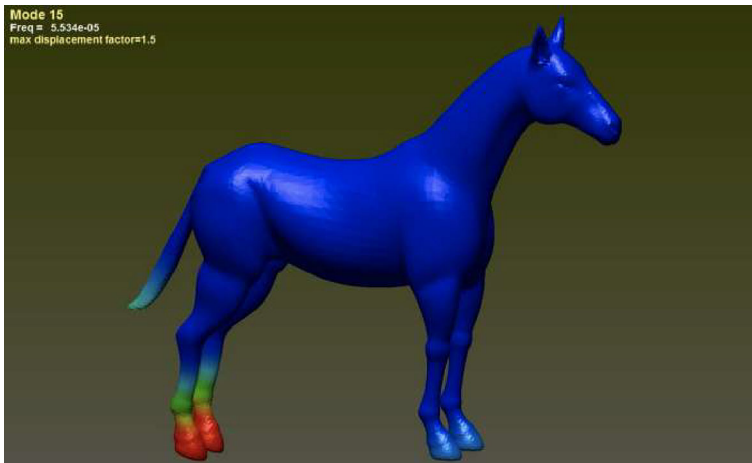
Fig. 20 This is Mode 15, showing an in-phase synchronous walking motion of the hind legs. There is also minor motion of the fore legs. For video animation, please click http://people.tamu.edu/~asergeev/presentations/pres-2022-09-02/horsem1-15/movie_015.mp4
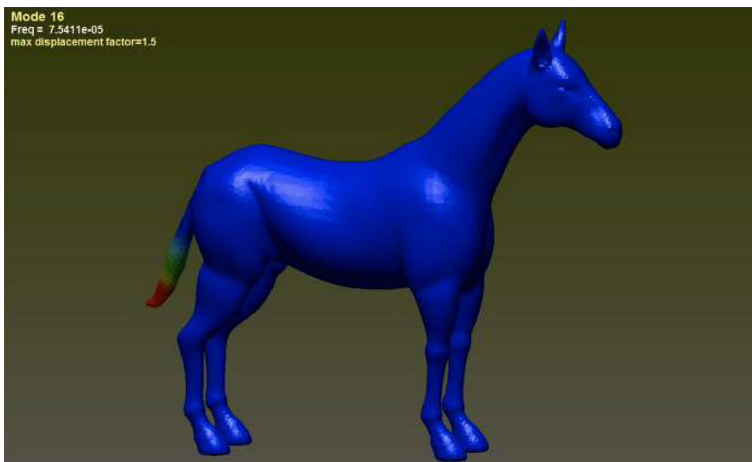
Fig. 21 This is Mode 16, showing side-to-side (left-and-right) wagging of the horse's tail. Note that the direction of wagging is perpendicular to that in Figure 15. Again, we interpret it as an economic way for a horse to communicate its mood to the master or to other horses. For video animation, please click https://drive.google.com/file/d/1fgXJ8DuKvyOIEplK5PKlYpyj9FAABEGj/view?usp=sharing

5.4.2 Local Motions of the Horse Head

The local motions of the head are collected and shown in Fig. 40. Please note that there are always accompanying motions on other parts of the horse.

5.4.3 Local Motions of the Horse Tail

The local motions of the head are collected and shown in the panels of Fig. 40.
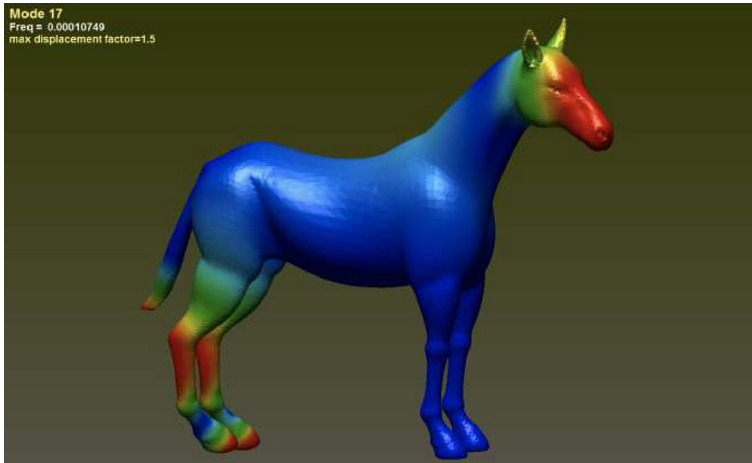
Fig. 22 This is Mode 17. It is the first mode showing three different rotations of the horse parts: the head, hind legs and tail. The hind legs show side-to-side bending motion, and this side-to-side motion is in phase with that of the head, while the tail's side-to-side wagging motion is out-of-phase with those of the hind legs and head. For video animation, please click https://drive.google.com/file/d/1x8QWpr3Wg3nswh8Bly_gzJdF-GfOlws1/view?usp=share_link
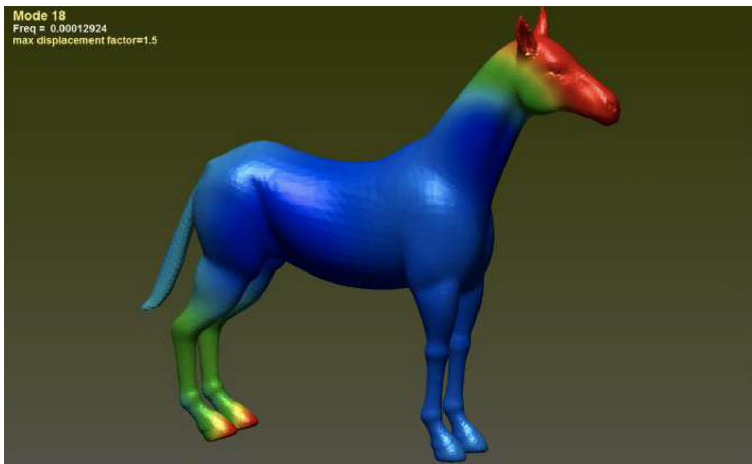
Fig. 23 This is Mode 18. It is showing the motion of two different parts of the horse: the head and hind legs. The hind legs are moving in phase up and down, and the head's up-and-down motion is in phase with the nodding of the head. For video animation, please click https://drive.google.com/file/d/1eFTBPHg-NoxKtz5pIcDvOy5BvgUPny_z/view?usp=sharing

6 Modal Analysis of Horse on a Floor

A horse may be carrying a rider or pulling a carriage. But its most important, and perhaps the *only* natural interaction with the environment, is the ground or floor that the horse is on. Therefore, in this section, we consider the modal analysis of a horse
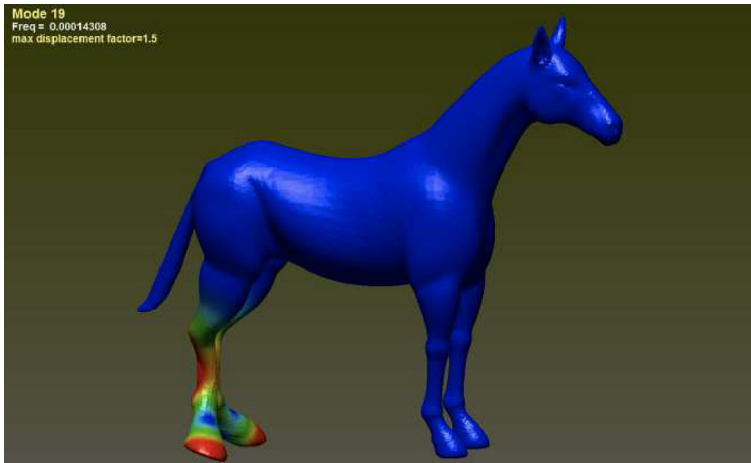
Fig. 24 This is Mode 19. It is showing the motion of symmetric rotating of the two hind legs opposite to each other. For video animation, please click https://drive.google.com/file/d/1fgJS0vmHaIEQy2fB8RgjZXQiDm58zRFE/view?usp=share_link
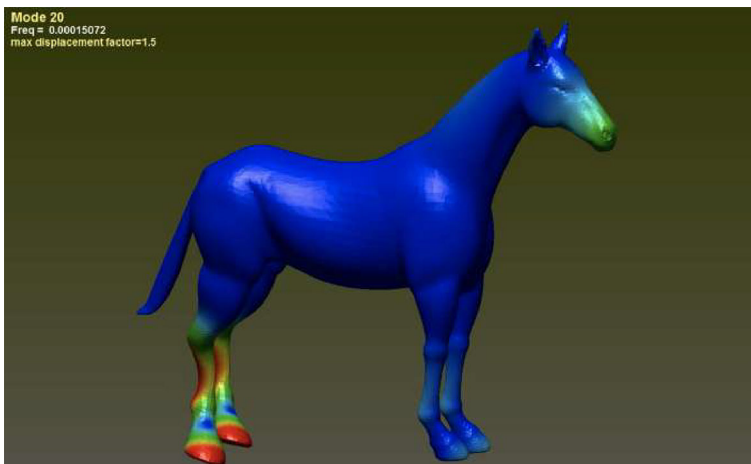
Fig. 25 This is Mode 20. The prominent motion is showing a rotating motion in the same orientation of the hind legs. There is also a side-to-side rotation of the head. The side-to-side motions of the leg rotation is in phase with that of the head. For video animation, please click https://drive.google.com/file/d/1WuGSdosLu89_kidE6Kb6CN7zP16C_zWF/view?usp=share_link

on floor. This is done by adding a contact condition on the hoofs/feet of the horse: the LS-DYNA keywords are (Figs. 41, 42, 43):

*CONTACT_ERODING_SINGLE_SURFACE

and

*CONTACT_AUTOMATIC_SURFACE_TO_SURFACE [19, pp. 11–51].

We have compiled the first 100 modes of a horse on a floor in the following:
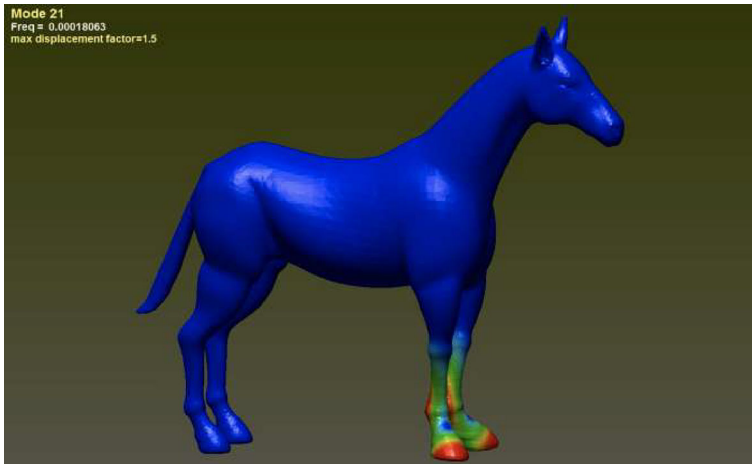
Fig. 26 This is Mode 21. The motion is showing a symmetric rotation of the fore legs in opposite orientations. For video animation, please click https://drive.google.com/file/d/11C7pps34_4_dEVLU4ajuI-rkZYTkIcDj/view?usp=sharing
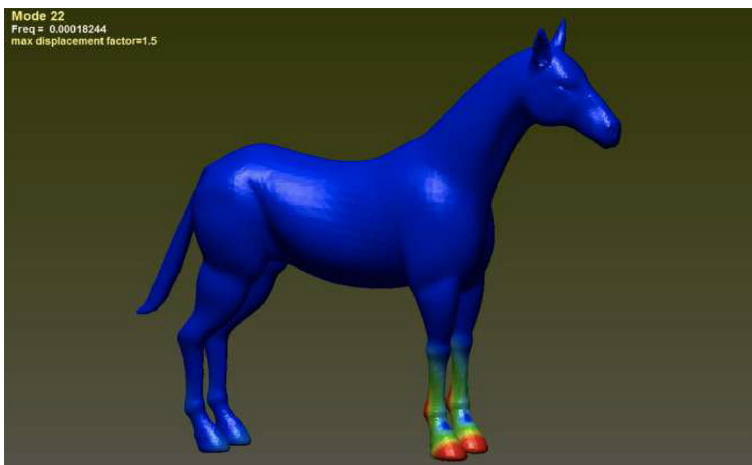
Fig. 27 This is Mode 22. The motion is similar to that of Mode 21, except that the fore legs are rotating in the same orientation. For video animation, please click https://drive.google.com/file/d/1wEqqR8QsT1twQRmd5jrv8OvyKYNTxR_o/view?usp=sharing

https://drive.google.com/file/d/1QlaLalBuKa-5jzSxa8NBOd9z5wHrdO3u/view?usp=share_link   (6.1)

Unsurprisingly, many of the mode shapes are quite similar to those of a horse without floor as shown in (5.1). Except that the sequential order of occurrences of such similar, look-alike modes may change. The major novelty here, however, is the effect of the floor as a constraint. In our opinion, such a constraint makes the motions more "sure-footed" and natural. Here, we are displaying some of such more natural-looking modes.
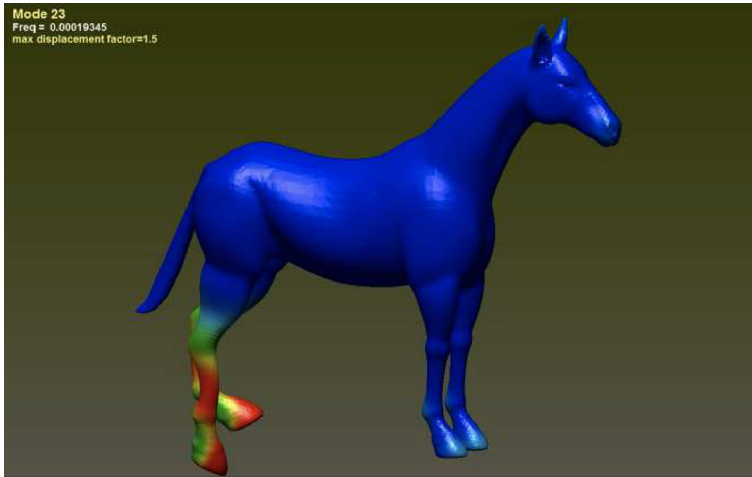
Fig. 28 This is Mode 23. The motion is showing an walk in alternating high-step motion of the hind feet. For video animation, please click https://drive.google.com/file/d/1SEn6mHxAAjF4AxVODnHyaEO6dyXUmPeB/view?usp=share_link
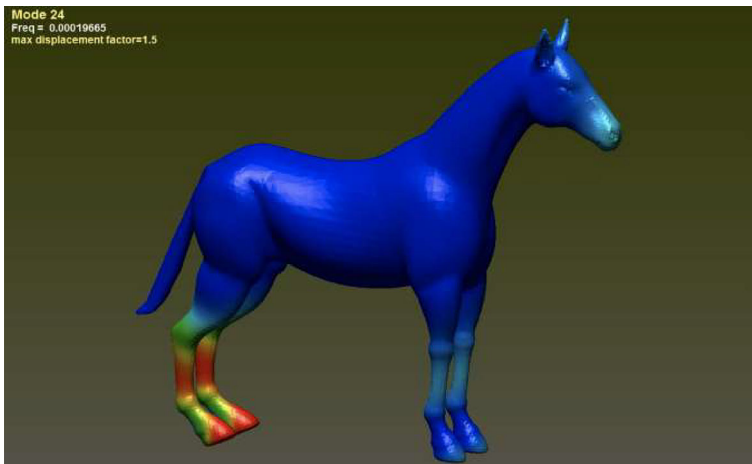
Fig. 29 This is Mode 24. The motion is showing a synchronous high-step motion of the two hind legs. There are also minor motion of the fore legs and the head, and the nodding motion of the head. For video animation, please click https://drive.google.com/file/d/1-HgJTrV0DtNQK3NWzgLhwsmVsUBlAJdW/view?usp=share_link

From Figs. 45 and 47, we see that a horse can perform pronk and bound motions. It can also perform pacing and trotting motions as such motions can be formed by linear combinations of Modes 13 (Fig. 44) and Mode 15 (Fig. 46). Despite this achievement, we must note that a horse can have many different gaits, which have not been captured by us. Only more study can enable us to make more findings about general horse gaits.

A tabulated interpretation of modes (up to mode #30) is given in Table 1.
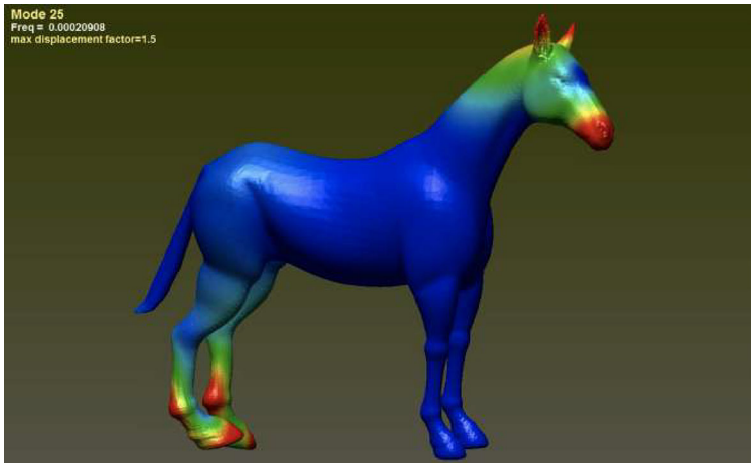
Fig. 30 This is Mode 25. The motion is showing a synchronous rotating motion of the two hind legs. There is also a minor out-of-phase side-to-side yawing motion of the head. For video animation, please click https://drive.google.com/file/d/1DfNOb_xRZ1E9a0l9BRkxHgsjOtNqNEKL/view?usp=share_link
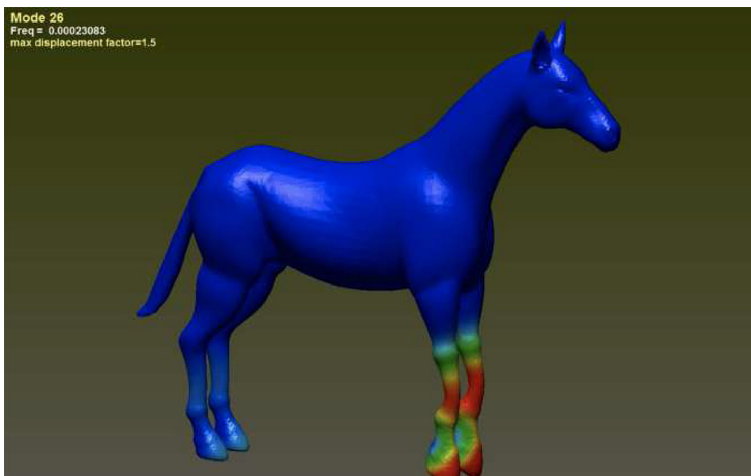
Fig. 31 This is Mode 26. The motion is showing two fore legs performing a synchronous high-step motion, and some minor motion of the two hind legs. For video animation, please click https://drive.google.com/file/d/1YZMh1-pya2p-XGb8zHRxqe_D5bAvPAkM/view?usp=share_link

7 Modal Analysis of a Camel

We now discuss the modal analysis of a camel, along similar parallel lines as we did for the horse in the preceding sections. As a result, we will be more concise.
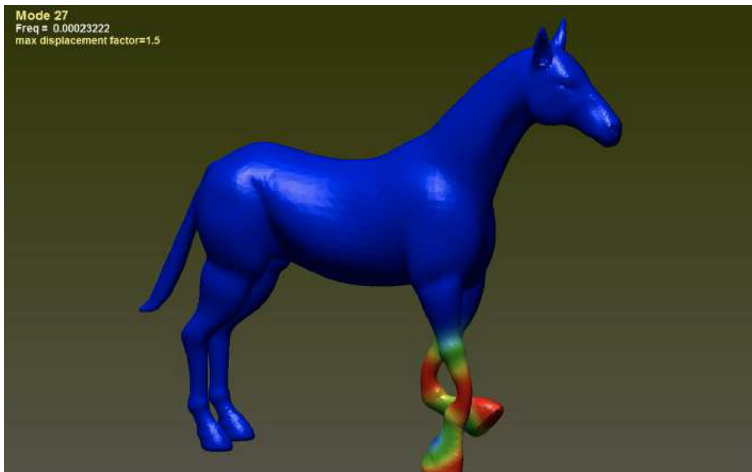
Fig. 32 This is Mode 27. It is showing an alternating high-step fore two legs motion. For video animation, please click https://drive.google.com/file/d/1yPixaNUvRxBifD-jXugaZtYHZLAWbn0-/view?usp=share_link
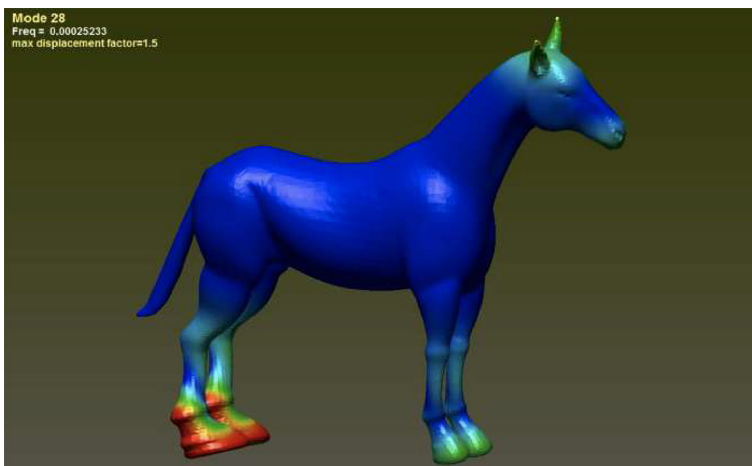
Fig. 33 This is Mode 28. The motion is showing a rotating and twisting, pairwise synchronous motion of the two hind legs. There is also a minor twisting and rotating motion of the fore legs out-of-phase with the hind legs. The head is also yawing in-phase with the hind legs. Note that the hind feet are "popping" or swollen. For video animation, please click https://drive.google.com/file/d/1WHinL5XZQaD8NOfhwVHyPqjQ2HBmEhiF/view?usp=sharing

7.1 The CAD Camel Model

Our 3D camel CAD model is taken from an online open-source resource Creazilla [26]. The mesh generation process is similar to that of the horse. Thus, we will not need to repeat the technical details.

The material and computational parameters are:

Number of finite elements	367,558
Number of nodes	72,364
Area	$1.45028e+07 \ mm^2$
Volume	$1.98963e+09 \ mm^3$
Mass	kg
Corrected material	
Density	$1.15e-6 \ kg/mm^3$
Young's modulus	$3.5e-6$ GPa
Poission's ratio	0.45
Yield stress	0.47 GPa
Tangent modulus	0.0
Hardening parameter	0.11
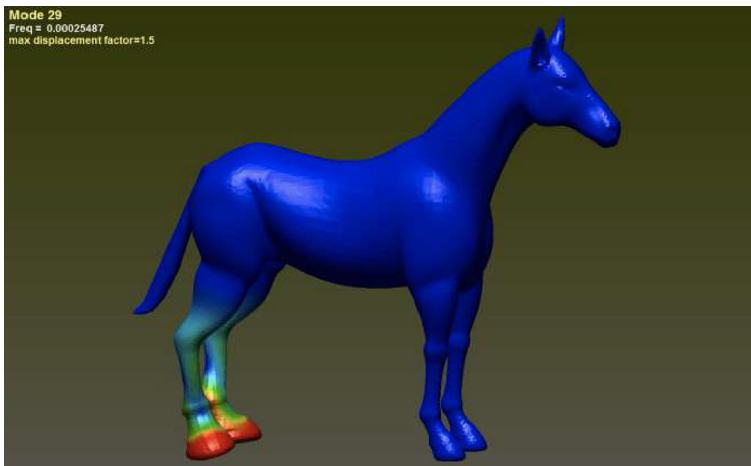
Fig. 34 This is Mode 29. The motion is showing a rotating and twisting, motion in opposite orientation of the two hind legs. The two hind feet are also swollen. For video animation, please click https://drive.google.com/file/d/1Td-HG9zdtIsFCQ-v-0tRQ-Ci6MdLOIpQ/view?usp=sharing
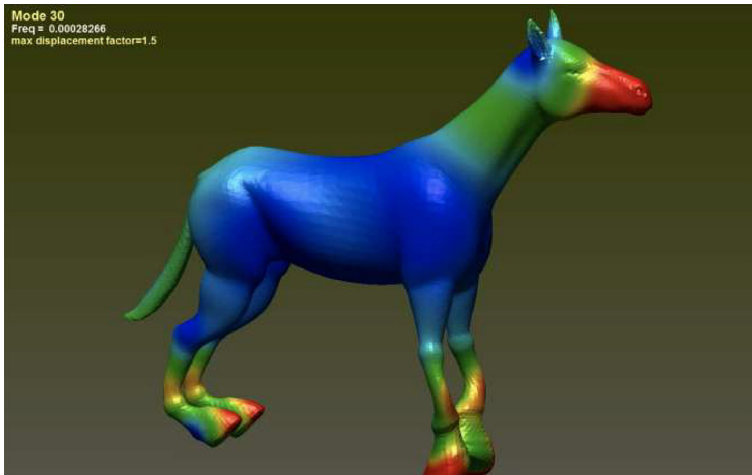
Fig. 35 This is Mode 30. The motion is showing a pairwise out-of-phase high-step motion of the two fore legs and the hind legs. The head is also pitching up-and-down out-of-phase with the fore legs. For video animation, please click https://drive.google.com/file/d/1Qm8ufSZF9nAHGm3gDYr4SC_r7byUk7na/view?usp=sharing
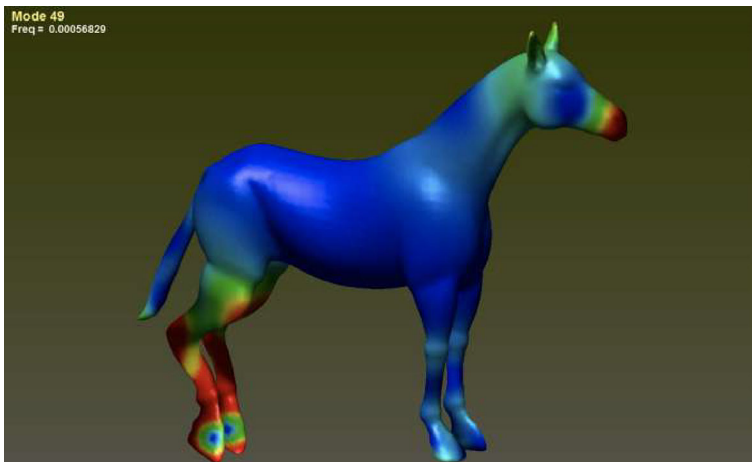
Fig. 36 This is Mode 49 in (5.1), where we see excessive bending, twisting and rotating of the lower portion of the hind legs. For video animation, please click https://drive.google.com/file/d/14o73sYsA8lkw_u_lFFIa9yBQdaBGVwGT/view?usp=sharing
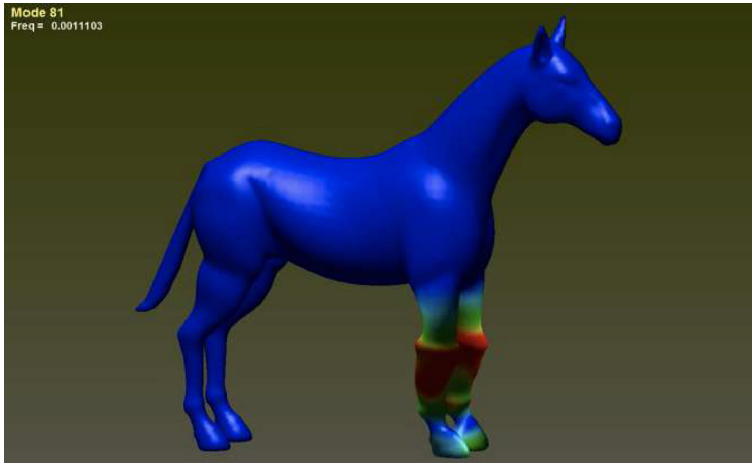
Fig. 37 This is Mode 81, where we see excessive popping and rotation of the joints of the fore legs. This could be an *injuring mode*. For video animation, please click https://drive.google.com/file/d/1O6XGDe1zzTDmGmQMq9VR_7WfRFOdTgjV/view?usp=sharing
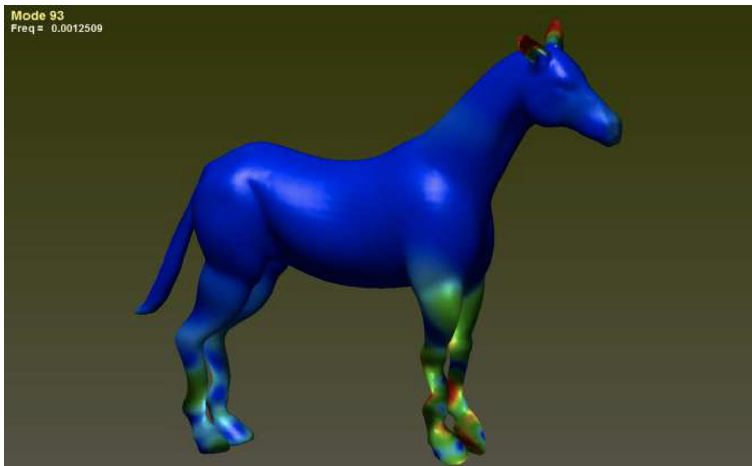
Fig. 38 This is Mode 93, where we see grossly oscillatory motion on the bent fore legs and joints. For video animation, please click https://drive.google.com/file/d/1QLZs0V0NvLcnKc74-U2r7kHDryV_P4RQ/view?usp=share_link
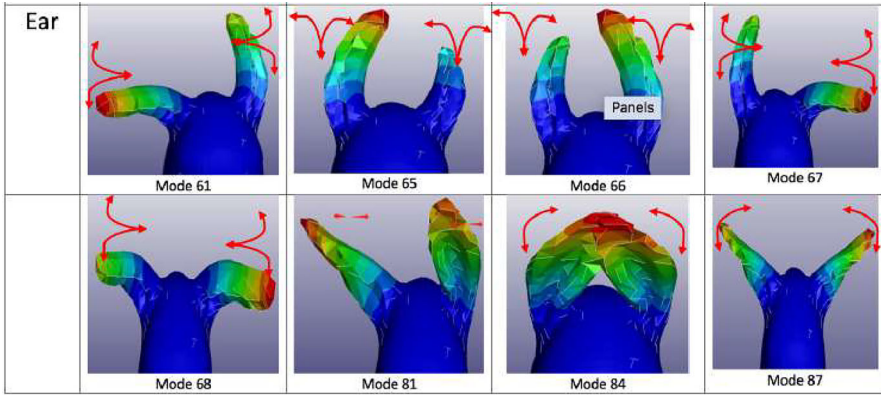
Fig. 39 This panel shows the motion patterns of the horse ears. These motions are local, i.e., there are no motions on other parts of the horse body. We believe they are related to the communications between horses or between a horse and its master
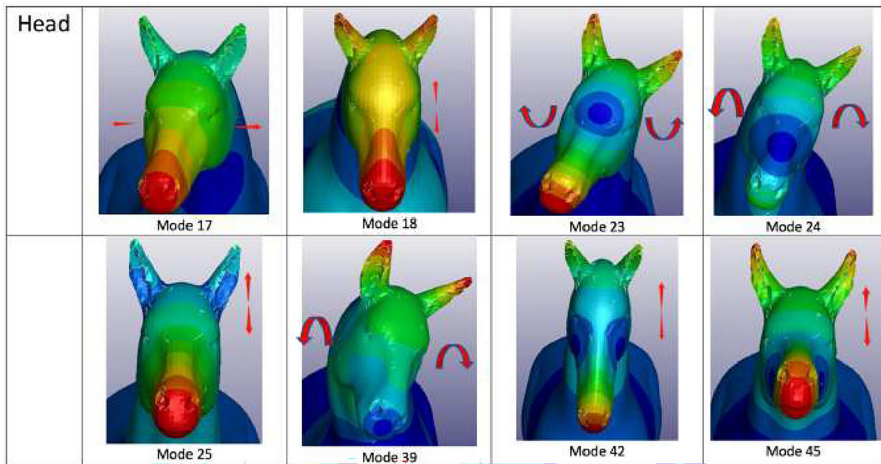

Fig. 40 This panel shows the motion patterns of the horse head. These motions are not local, i.e., there are certain motions on other parts of the horse body. We believe the motions of the head are related to the communications between horses or between a horse and its master, or, sometimes, between the balancing of the body in motion as the motions are not local
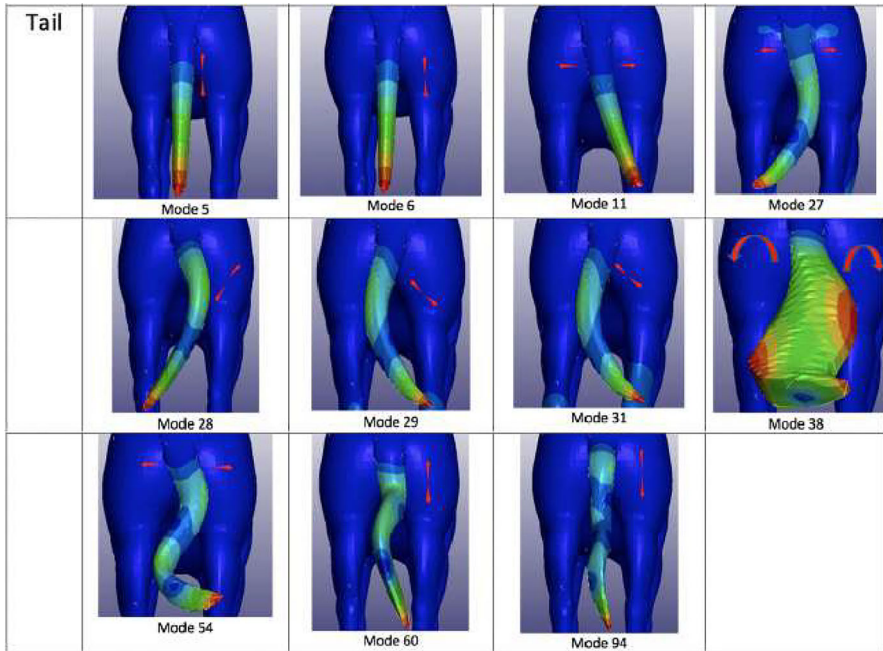
Fig. 41 This panel shows the motion patterns of the horse tail. These motions are local, i.e., there are no motions on other parts of the horse body. We believe the motions of the tail are related to the communications between horses or between a horse and its master
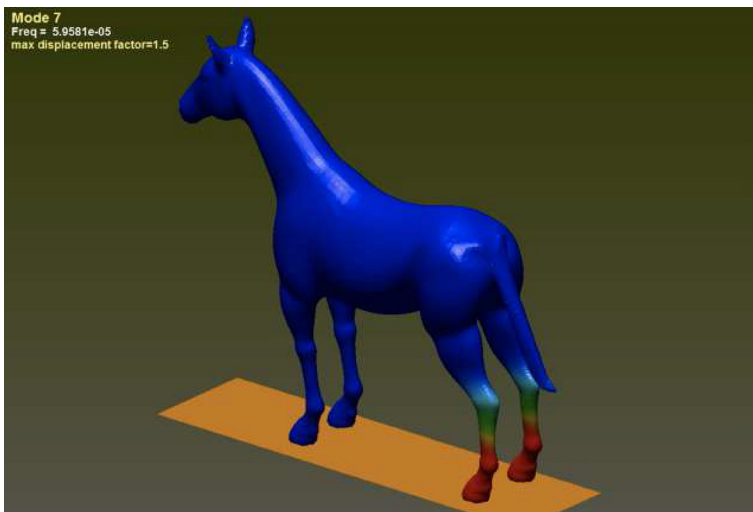
Fig. 42 This is Mode 7 in (6.1), where we see the lateral in-and-out motion of the hind legs. For video animation, please click https://drive.google.com/file/d/19EClGdhnQjYlBOx6E-1nNF3_-ZwVbCuz/view?usp=sharing
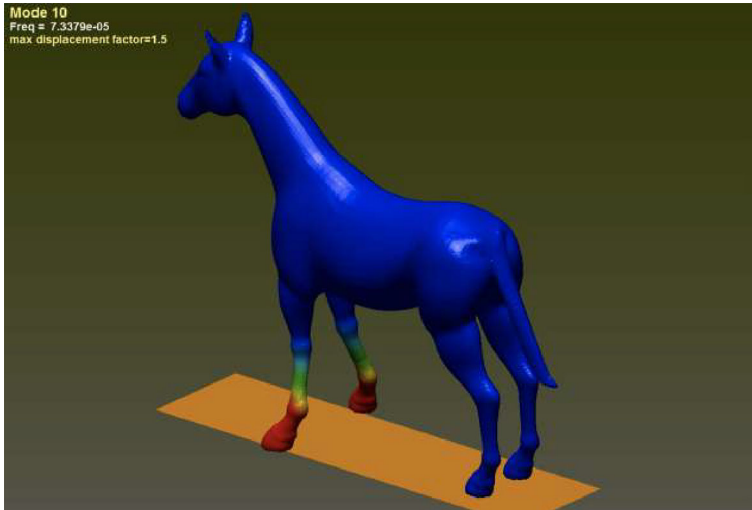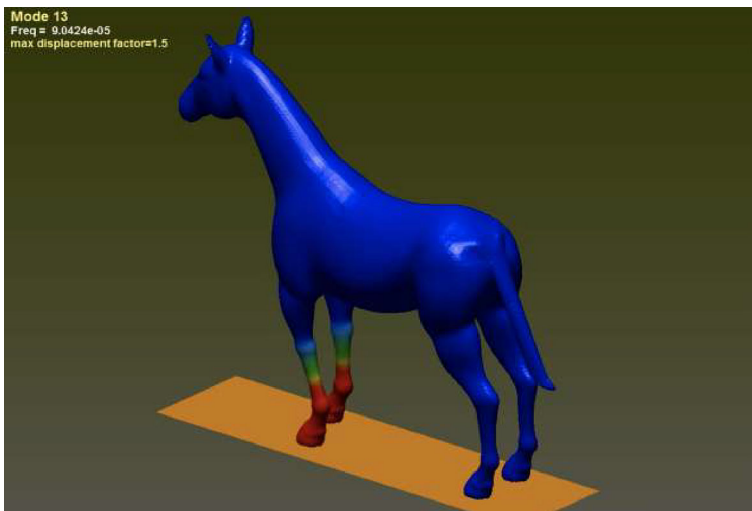
Fig. 43 This is Mode 10 in (6.1), where we see the in-and-out lateral motion of the fore legs. For video animation, please click https://drive.google.com/file/d/1e8fii1fM-6x-msteP78isJd6MbkiOmBf/ view?usp=sharing

Fig. 44 This is Mode 13 in (6.1), where we see the walking/pacing motion of the fore legs. For video animation, please click https://drive.google.com/file/d/1MT-S0OPtFY7A0ambkHL1gvPe5ZWq2kls/view? usp=sharing
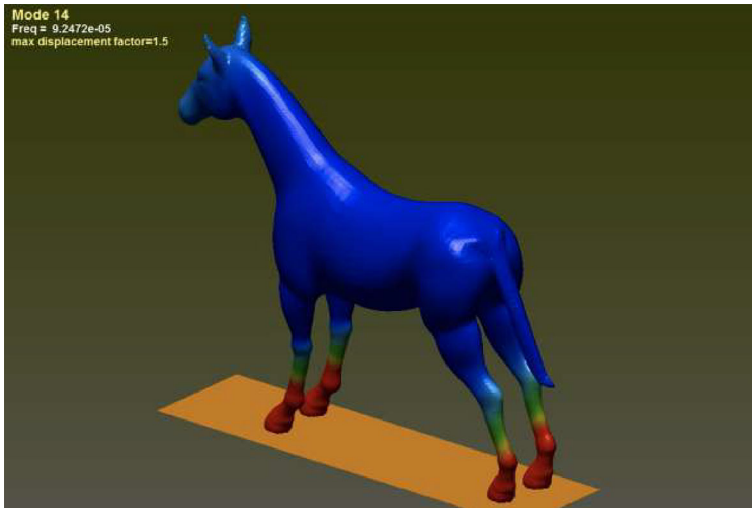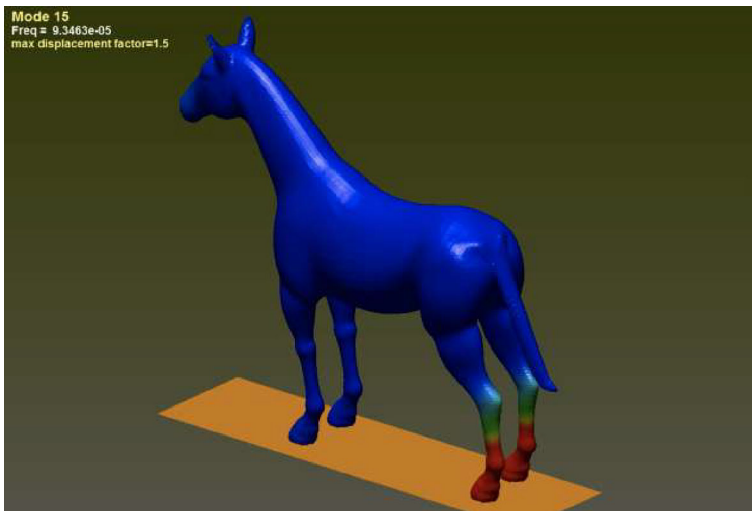
Fig. 45 This is Mode 14 in (6.1), where we see the bounding type cantering/galloping motion of the horse. For video animation, please click https://drive.google.com/file/d/1ukKrmZO0G3fMURFcFEc0WJIgKA3rtMP0/view?usp=sharing

Fig. 46 This is Mode 15 in (6.1), where we see the walking/pacing motion of the hind legs. For video animation, please click https://drive.google.com/file/d/1OHwZ-DETZiisoYr5hxEQhUq2kynzWt34/view?usp=sharing

Table 1 Interpretation of the first 30 modes of a horse on floor

| Mode#	Mode name	Interpretation
1, 2, 3	Rigid body motion	Rotate and forward motions of the horse
4	Rocking motion of the horse	Rock motion
5	Lifting of the fore legs and (up-down) tail wagging	Communication
6	(up-down) Tail wagging	Communication
7	Side-to-center hind leg movement	Unclear (unspecific leg movement)
8	Out-of-phase rocking of the fore legs and hind legs	Unclear (unspecific leg movement)
9	Side-to-center motion of fore legs	Unclear (unspecific leg movement)
10	Left-right tail wagging	Communication
11	Left-right movement of the fore legs	Making turns
12	Out-of-phase two fore legs motion	Walking/pacing
13	Out-of-phase movement of the pairs of fore and hind legs	Bounding
14	Out-of-phase motions of the hind legs	Walking/pacing (together with Mode 13)
15	Out-of-phase movement of the pairs of fore and hind legs	Pronking
16	Left-right head motion, whole body motion	Communication, shaking of body
17	Up-down body motion	Communication
18	Hind lower-leg twisting (symmetric)	Unspecified leg motion
19	Hind lower-leg twisting (antisymmetric)	Unspecified leg motion
20	Fore lower-leg twisting (symmetric)	Unspecified leg motion
21	Fore lower-leg twisting (antisymmetric)	Unspecified leg motion
22	Yawing of head and hind legs rotating	Communication (while leg motion is unspecific)
23	Head yawing and leg twisting	Communication (while leg motion is unspecific)
24	Head nodding and leg twisting	Communication (while leg motion is unspecific)
25	Hind legs twisting	Unspecified leg motion
26	Tail wagging	Communication
27	Tail wagging	Communication
28	Tail twirling	Communication
29	Tail twirling	Communication
30	Tail twirling and legs movement	Communication; unspecified body movement
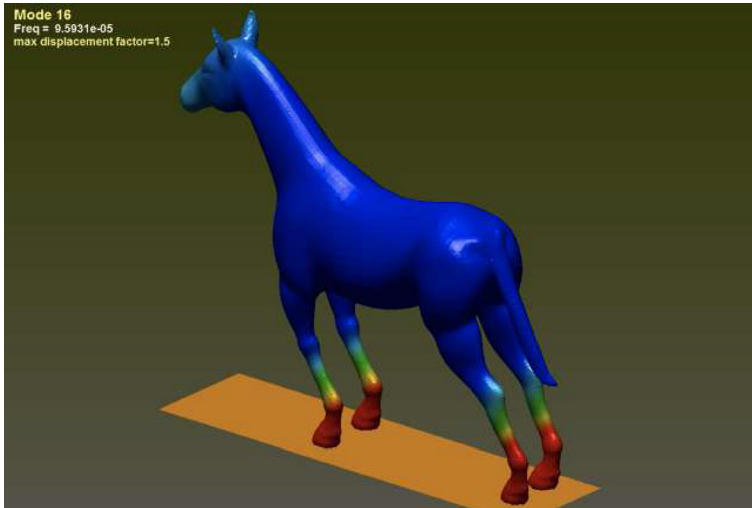
Fig. 47 This is Mode 16 in (6.1), where we see the pronking type cantering/galloping motion of the horse. For video animation, please click https://drive.google.com/file/d/1hybAP5dcWwayDqJsD1ZhTAiZa9Zcl9z2/view?usp=sharing
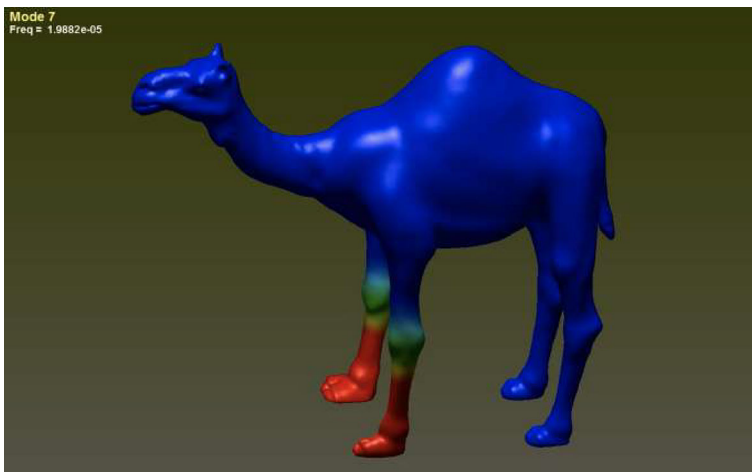

Fig. 48 This is Mode 7 in (7.1), the first non-rigid body motion of camel, showing a synchronous in-and-out lateral motion of the two fore legs. There is also some minor motion of the hind legs, For video animation, please click https://drive.google.com/file/d/1mPAzajBlrGXsGcrHB6TOx4MpzQzQP1tL/view?usp=sharing

In https://drive.google.com/file/d/1RiFR05DQWvSdjGok3GGOe6ORjk7xsiFB/view?usp=share_link,   (7.1)

we display the first 100 modes. Their frequencies are tabulated in the Appendix.
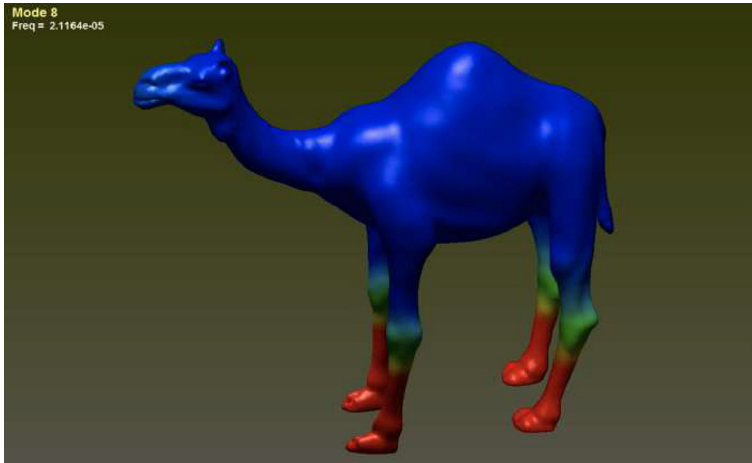
Fig. 49 This is Mode 8, which is the same motion as in Mode 7, except that here the lateral motion happens on, respectively, both the fore and hind legs, out-of-phase. For video animation, please click https://drive. google.com/file/d/1zY1cQWFv9I2hNmy6Ged_GMbaAOPalWWf/view?usp=sharing
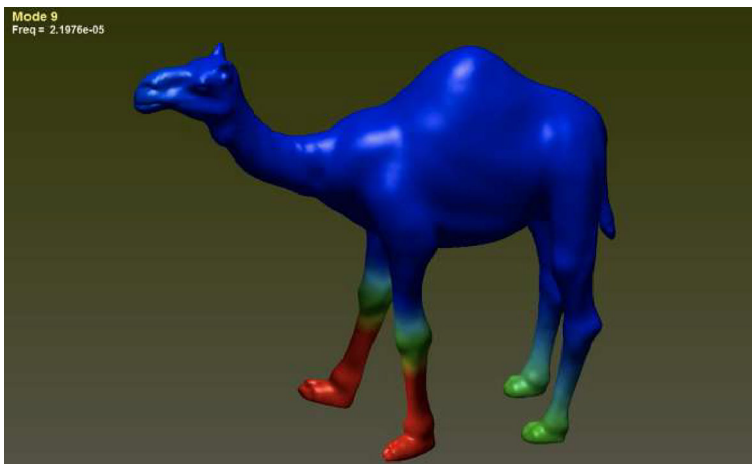

Fig. 50 This is Mode 9. Here the prominent is the back-and-forth (i.e., forward-and-backward) walking motion of the fore legs. There is also minor motion on hind legs of the camel. For video animation, please see https://drive.google.com/file/d/11VpFVsRzW9P-CtXtVF8xu_WTaVJyUh0n/view?usp=sharing

7.2 Discussion of the First 100 Modes of a Camel (1): Without Floor

We first note that the first six modes are linear combinations of the six rigid-body motions as given in Sect. 3. So we begin from the seventh mode in (7.1) (Figs. 48, 49, 50, 51, 52, 53, 54, 55, 56, 57, 58, 59, 60, 61, 62, 63, 64, 65, 66, 67, 68, 69, 70, 71).
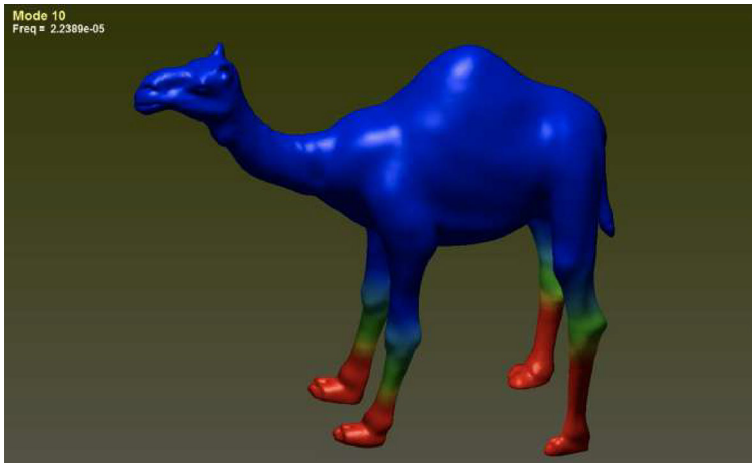
Fig. 51 This is Mode 10. This shows a 4-legged motion, where the two fore legs are moving back-and-forth, while the two hind legs are moving side-to-center. These directions of the two types of motion seem to be "orthogonal" to each other. For video animation, please click https://drive.google.com/file/d/1UwxKQ_Pxj4sP62hdiiwPZI_FzztcMB7D/view?usp=sharing

Fig. 52 This is Mode 11. This shows again a 4-legged motion, where the two fore legs are moving back-and-forth, while the two hind legs are moving laterally side-to-center. But the relative motion between the fore and hind legs are out-of-phase in comparison with that of Fig. 51. Once again, these directions of the two types of motion seem to be "orthogonal" to each other. For video animation, please click https://drive.google.com/file/d/1LpaYxuSA46AnyLGU8D4X6jgoaeChD58c/view?usp=sharing

7.3 The First 100 Modes of a Camel (2): With Floor

We compile and connect the first 100 modes in a video as follows:
https://drive.google.com/file/d/1HwetaCx1nHLyx6BnK1WF1luntc5AGO_q/view?usp=share_link   (7.2)
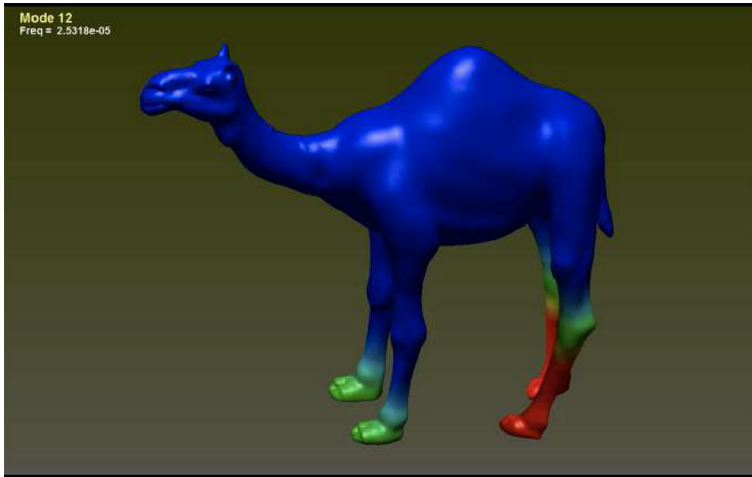
Fig. 53 This is Mode 12. It shows the walking, back-and-forth, motion of the hind legs. For video animation, please see https://drive.google.com/file/d/1zugX1JPIx7PXvX9AcFYYJyXWiyRQFkR3/view?usp=sharing
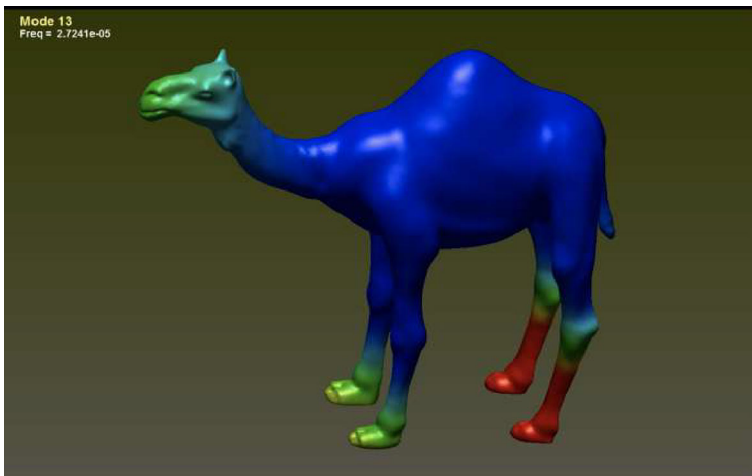

Fig. 54 This is Mode 13. Here the camel is in a "rocking" motion. The more prominent motion occurs on the hind legs. There is also minor in-phase motion on fore legs. For video animation, please see https://drive.google.com/file/d/1zJQQwDlWOhy2WSnBnbXKRGLWJiOtsF-o/view?usp=sharing

We noted earlier in Sect. 6 that the presence of floor makes the motion look more "sure footed". Here, like in Sect. 6, we mainly emphasize the modes related to camel's gaits.
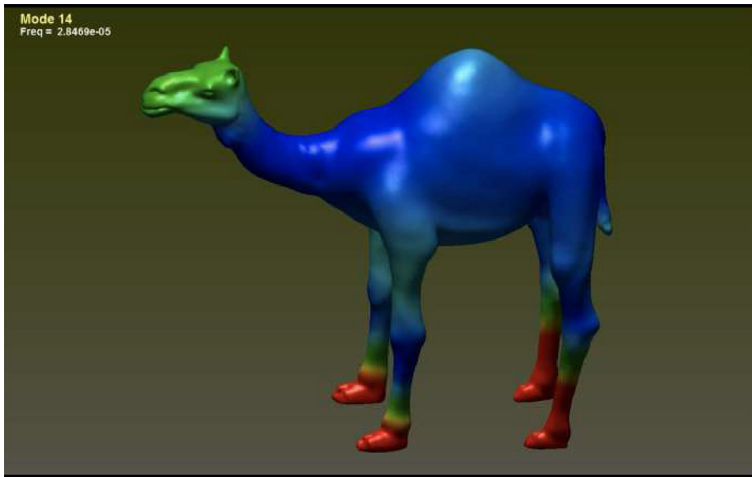
Fig. 55 This is Mode 14. Here the camel's fore pair and hind pair legs are rotating left-to-right in synchrony. For video animation, please see https://drive.google.com/file/d/1CP0NLnUhRkHboRGyn-NoQvzP-kxPtNBn/view?usp=sharing
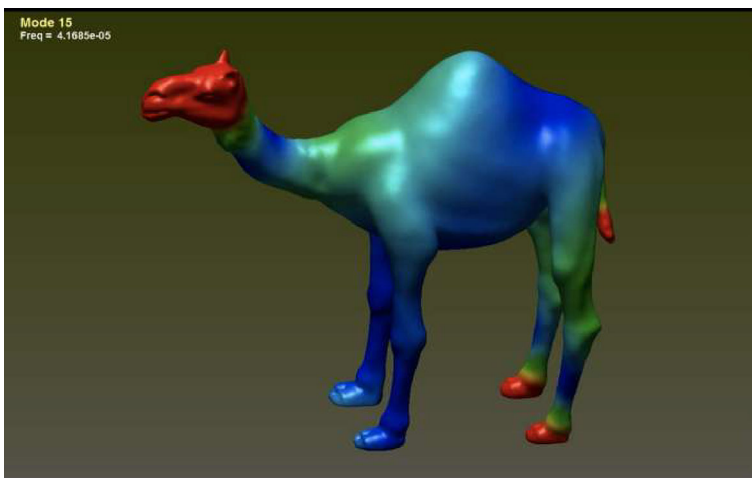

Fig. 56 This is Mode 15. Here the major motion is the synchronous left-to-right yawing of the head and tail. There is also some minor motion of the legs. For video animation, please see https://drive.google.com/file/d/1d9_eulsHXXgO5IsSFU2SVjQCm4UKo_Pp/view?usp=sharing

7.4 Comments on Some Higher Frequency Modes of a Camel

In Sect. 5.3, for the horse we have noted the fact that, as the mode number gets higher, the likelihood that the mode becomes spurious and unrealistic increases. For the camel, the situation is similar. The reader can see the video in (7.1) to verify for him- or herself. Thus, there is no need to add graphics or videos similar to those as shown in Figs. 36, 37 and 38 so as to avoid repetition.

Fig. 57 This is Mode 16. Here the major motion is the up-and-down pitch of the head. There is also some minor up-and-down motion of the fore and hind legs, and that of the tail. For video animation, please see https://drive.google.com/file/d/1KX096q_A43kTUsN_-ccuAHo0OxylhKOT/view?usp=sharing
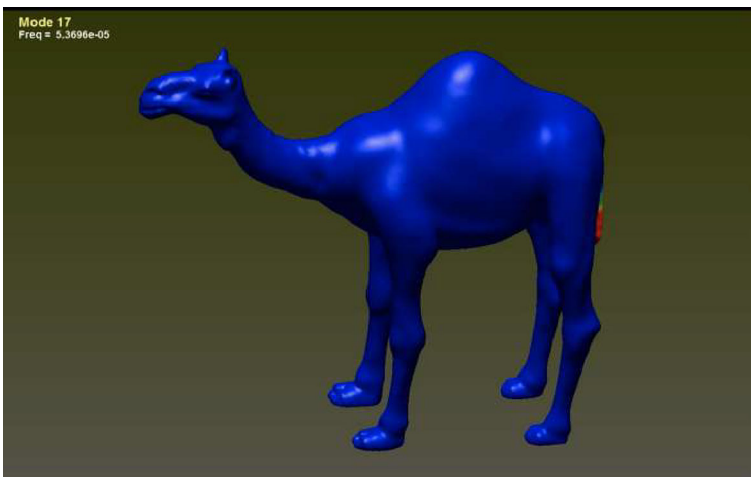

Fig. 58 This is Mode 17. Here, the major (and only) motion is the up-and-down pitch of the tail. For video animation, please see https://drive.google.com/file/d/1aWTpcVi5kP36oGTF4NgLmnqUU8Zcu-Mg/view?usp=sharing

Nevertheless, here, we add one higher order mode related to the camel's *hump*, which is unique to the camel, as an example of a characteristic of the camel in Fig. 72.

Remark 3 Modes 10 and 11 as shown, respectively, in Figs. 73 and 74 seem to indicate that their linear combinations can form the trot gait. But the trot gait for a camel has never been observed. The only walking gait for a camel is the pacing (syncopated walk) motion. This is a puzzle we still have not been able to answer (Figs. 75, 76, 77).
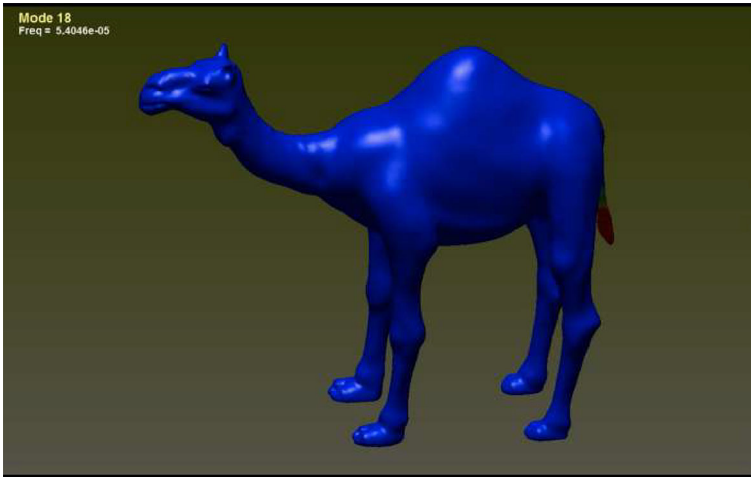
Fig. 59 This is Mode 18. Here, the major (and only) motion is the left-to-right wagging of the tail. For video animation, please see https://drive.google.com/file/d/1ffs9mzMyX4F2_8GlBKwDlNXPFfj_MUdQ/view?usp=sharing
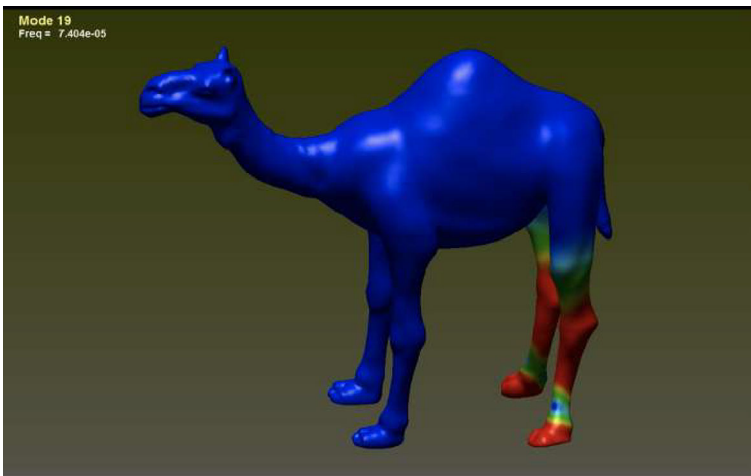

Fig. 60 This is Mode 19. Here the motion is the rotation, in opposite orientation, of the lower hind legs. For video animation, please see https://drive.google.com/file/d/1V0f_FUFLZwFfJuDr3lHnRXZGLKvg216w/view?usp=sharing
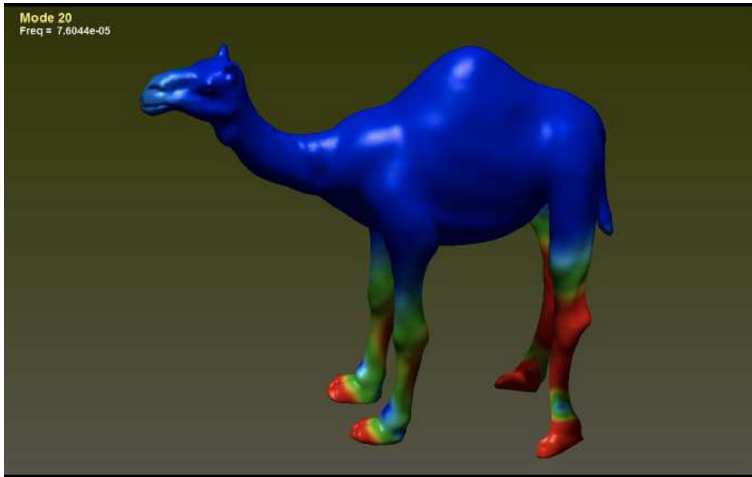
Fig. 61 This is Mode 20. Here, the hind legs is tramping with rotation of the hind feet in opposite orientation. There is also some minor rotational motion of the fore legs, but with the same orientation. For video animation, please see https://drive.google.com/file/d/15UB8Dexz-QONlCPKTepfXgqIjEyyo-8R/view?usp=sharing
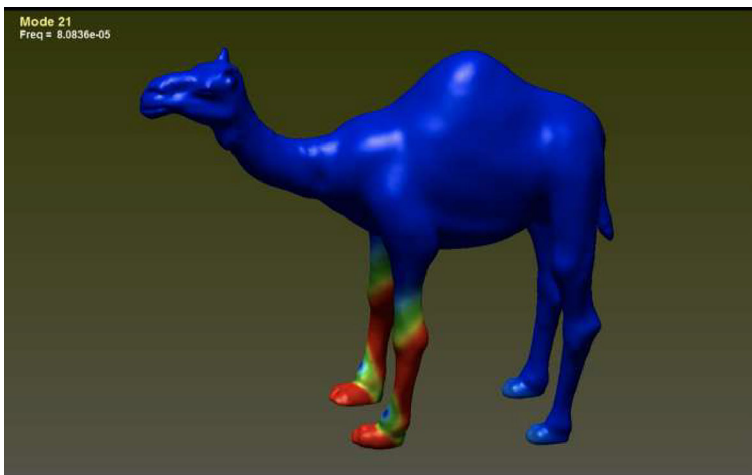

Fig. 62 This is Mode 21. It shows the rotation of the lower-half fore legs in opposite orientation For video animation, please see https://drive.google.com/file/d/1GsI--EzC53tbg0N4NdqQiY0Eqxxv7VcW/view?usp=sharing
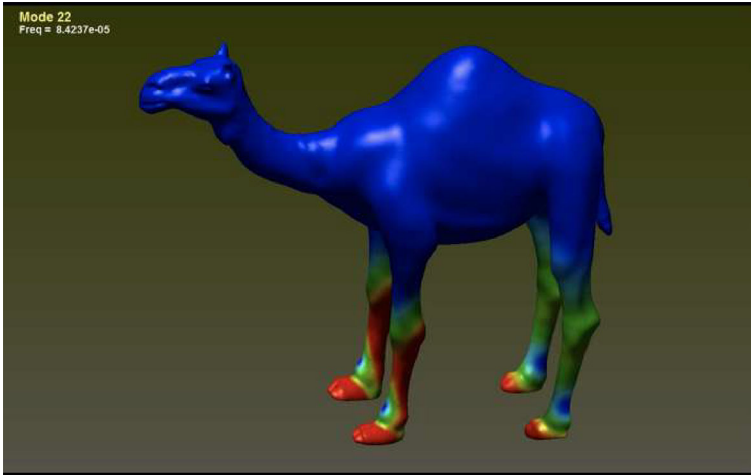
Fig. 63 This is Mode 22. The major motion is the rotation of the lower-half fore legs in the same orientation There is also a minor motion of tramping of the hind legs. For video animation, please see https://drive. google.com/file/d/1VjWQc2eGZomIZo7jMbAXSsCvIc5sxso5/view?usp=sharing
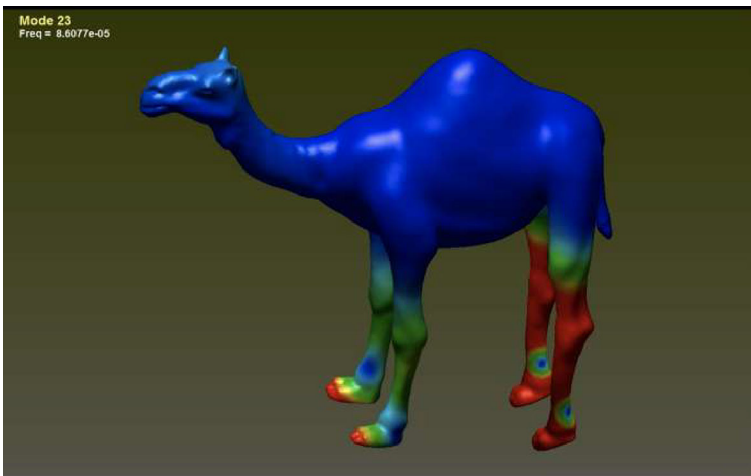

Fig. 64 This is Mode 23. The major motion is the step-up motion of the hind legs. There is also a minor bending motion of the fore legs. For video animation, please see https://drive.google.com/file/d/ 109fSzEuJs2_FBsz3fgSD1M-Zq5HO7qfY/view?usp=sharing

Fig. 65 This is Mode 24. The major motion is the tramping of the hind legs. There is also a minor rotation of the fore feet in the same orientation. For video animation, please see https://drive.google.com/file/d/1QO3Qcv3rkEvTc8M-9RdEiJ7Cf7TWvSw9/view?usp=sharing

Fig. 66 This is Mode 25. It shows the tramping of the fore legs. For video animation, please see https://drive.google.com/file/d/1t767dZMRUKFA_PxVFjs_K5AEv1dRzBoG/view?usp=sharing

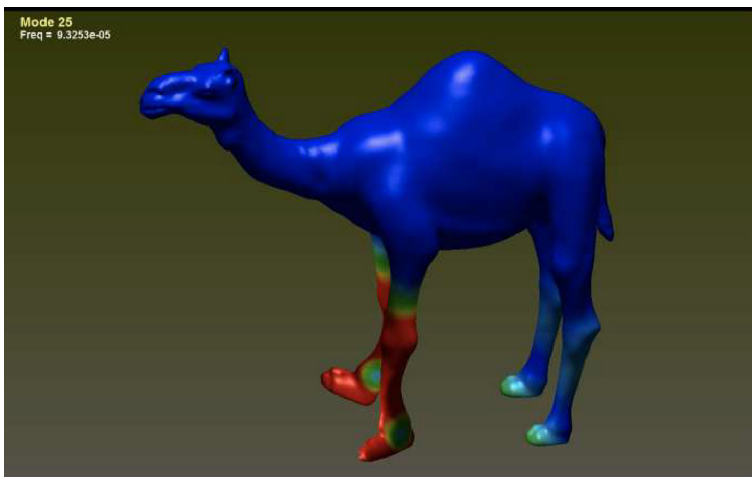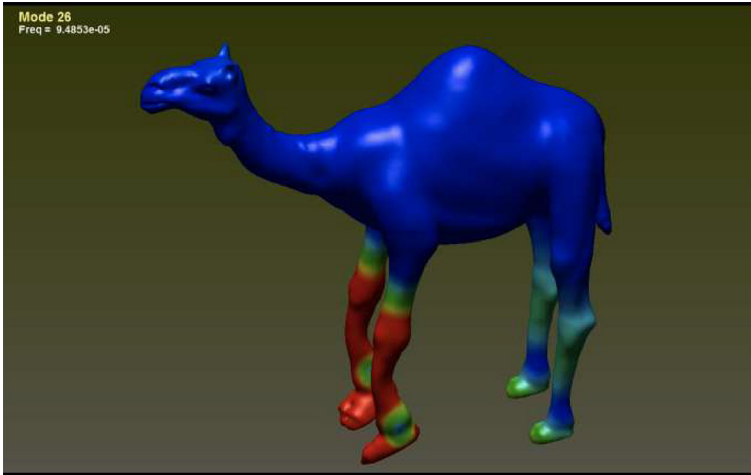**Fig. 67** This is Mode 26. It shows the step-up motion of the fore legs. For video animation, please see
https://drive.google.com/file/d/1yyEE7OTJ1bu6YYKpoXLN6wZ4fJ6CJIVx/view?usp=sharing
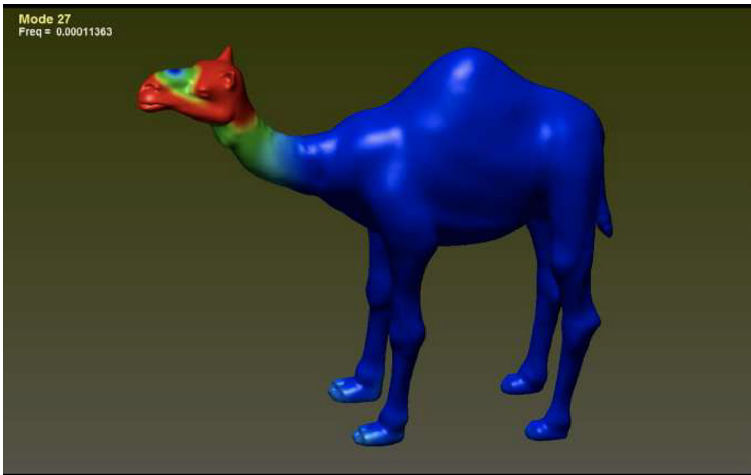
Fig. 68 This is Mode 27. It shows the neck-twisting motion of the head. For video animation, please see
https://drive.google.com/file/d/1qEzo-srYFl2Cwv8KN05OFqpExqVzywu1/view?usp=share_link
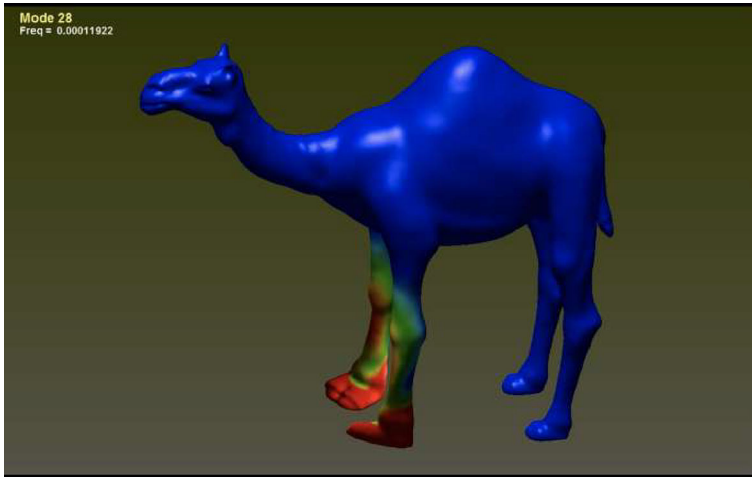
Fig. 69 This is Mode 28. It shows the twisting motion of the lower fore legs in opposite orientation. For video animation, please see https://drive.google.com/file/d/1SdlmRjvmOUf08xGAYQbFzln7ptQV3aG9/view?usp=share_link
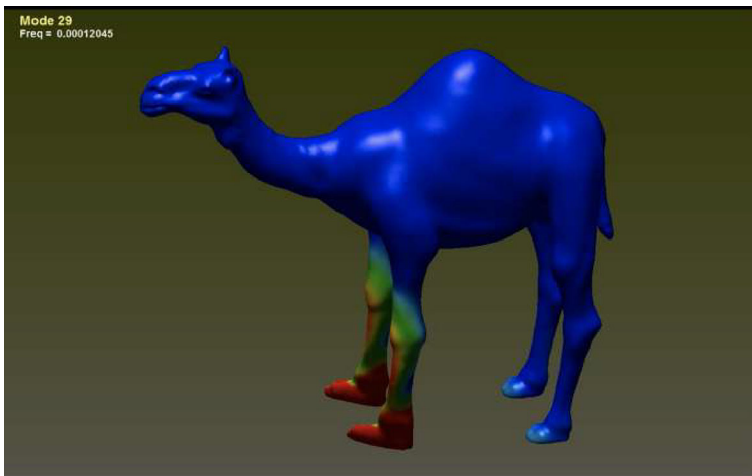
Fig. 70 This is Mode 29. It shows the twisting motion of the lower fore legs, but in the same orientation. For video animation, please see https://drive.google.com/file/d/1Wa26B9TeocTtvcFYsmlqnXp6gJNl-KlW/view?usp=sharing
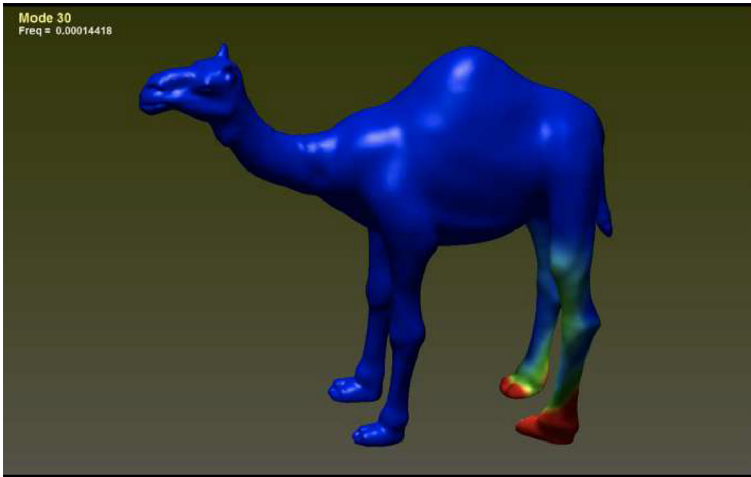
Fig. 71 This is Mode 30. It shows the twisting motion of the hind feet in the opposite orientation. For video animation, please see https://drive.google.com/file/d/1r8saIYOtDOdZOn8IMQWJscaSCWha2W2D/view?usp=sharing

Fig. 72 This is Mode 74. This is a full-body motion of a camel, where the movement of the camel's hump is quite noticeable. For video animation, please see https://drive.google.com/file/d/1MhrqVgWaxlUG6__vtMUMCsgV5RO0lFcf/view?usp=sharing
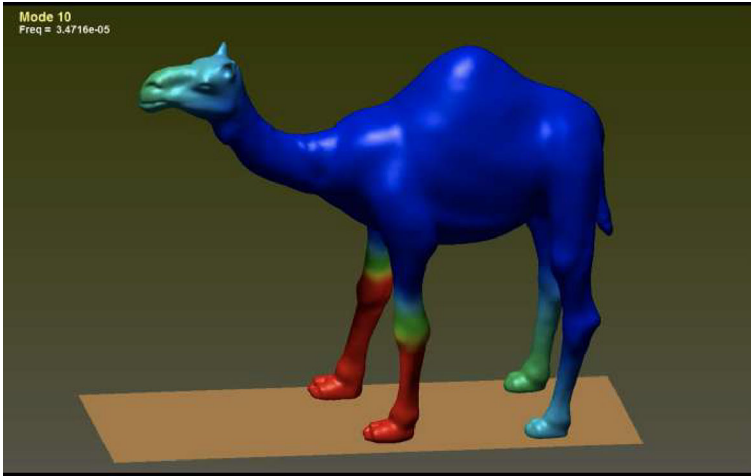
Fig. 73 This is Mode 10 in (7.2). It shows the walking/pacing, out-of-phase motion of the two fore legs. For video animation, please see https://drive.google.com/file/d/1-Myzgrdt4qiuEFYa6xZytfsLz3WB-5AW/view?usp=sharing
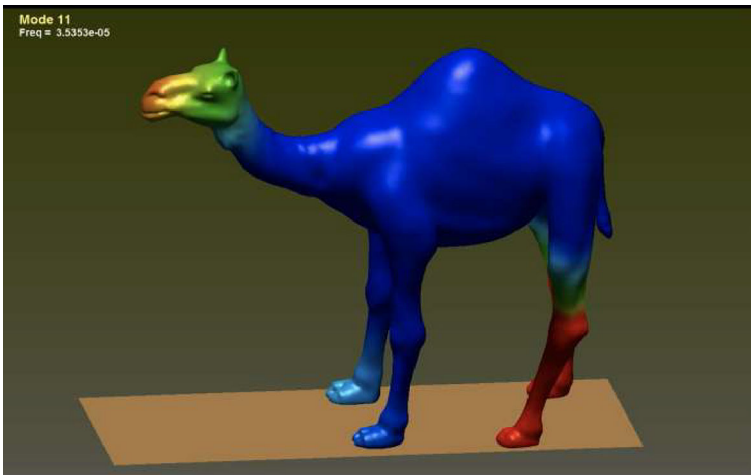
Fig. 74 This is Mode 11 in (7.2). It shows the walking/pacing, out-of-phase motion of the two hind legs. For video animation, please see https://drive.google.com/file/d/1O4IkkZnTEk9ZLe9rDF21NJhse2CmuPDs/view?usp=sharing

Fig. 75 This is Mode 12 in (7.2). It shows the pronk motion of the camel. For video animation, please see https://drive.google.com/file/d/1nnnKzlbXYzpKzuLkboWtFeZN3t9rx1VY/view?usp=sharing
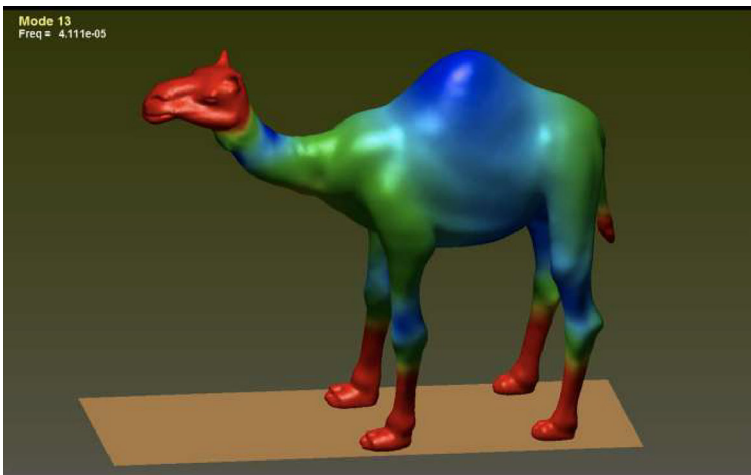
Fig. 76 This is Mode 13 in (7.2). It shows the pacing motion of the camel. This walk is often referred to as a syncopated walk, or a camel walk, due to a camel's usual walk gait where two legs move almost exactly at the same time, followed by the other two legs. For video animation, please see https://drive.google.com/file/d/12iBLzKBpvYiH8HN_zKlPuRFaffAB7ahd/view?usp=sharing

The *breathing mode* is quite common among animals. Here we include the following as an example in Fig. 78.
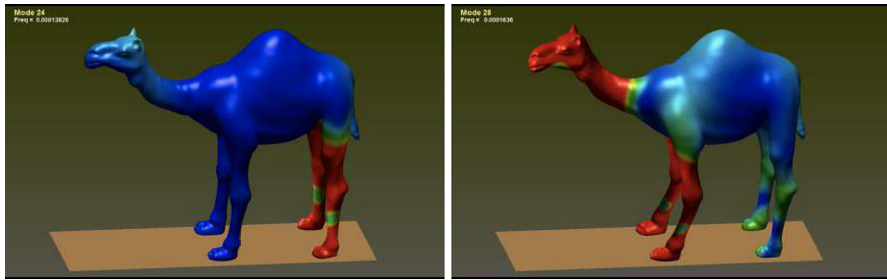
Fig. 77 Here we include both Modes 24 (left panel) and 28 (right panel) together. The former and latter can form linear combinations that become either pace or trot gaits. This again becomes puzzling as noted in Remark 3. For video animations, please click (for Mode 24) https://drive.google.com/file/d/1o-2AmOHjFJwpw-aULgLR-y5ifxjhYHdX/view?usp=sharing (for Mode 28) https://drive.google.com/file/d/1P5A8HZ9n0hqk6Ss1GI72F13oAa19bZAx/view?usp=sharing

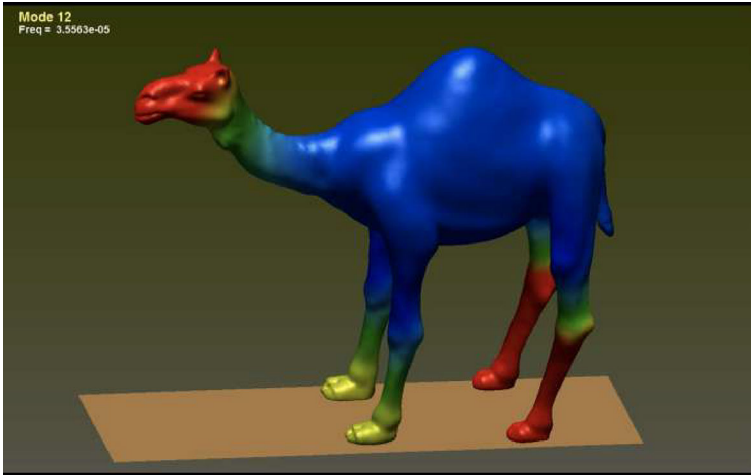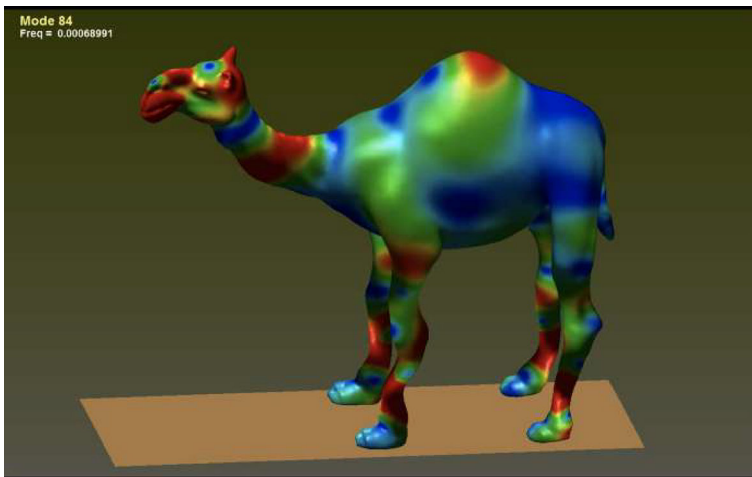**Fig. 78** This is Mode 84 in (7.2). It shows a breathing mode of the camel. For video animation, please see https://drive.google.com/file/d/18GcKCuSta6_j4s6ZszhyeDDnEkoyhDaD/view?usp=sharing

8 Concluding Remarks

We start this series of papers by using linear elasticity as the first step of computer modeling for animals. For the modeling to be as faithful and realistic as possible, there are numerous issues involved. Such issues are either currently beyond our capabilities and knowledge, or somewhat out of the scope of the main lines of interest. But they need to be further addressed. Here, we briefly describe some of them:

(i) For the contact condition between two geometrical objects, LS-DYNA offers some ten types of different possibilities of treatments. Our choice is
*CONTACT_SURFACE_TO_SURFACE
for the contact between the animals with the floor [27]. Due to the lack of further technical descriptions of this subroutine, we have essentially treated this contact as a "black box".

The simplest possible type of contacts is a quadratic programming problem with a linear constraint in a Hilbert space which, after discretization, becomes again a quadratic programming problem with a linear constraint in terms of nodal values. LS-DYNA's handling of such a nonlinear programming problem with constraints is by a penalty approach. However, it is unclear to us in the computation of modal analysis with contact constraints whether such a penalty algorithm is just linearized to yield the modal solutions.

(ii) We have quoted the famous book *"On Growth and Forms"* [28] by D'Arcy Wentworth Thompson. Regarding biological growth (and beyond), a set of notable mathematical papers have already been published in the contexts of finite elasticity and nonlinear PDEs. We refer the reader to [29–31] and the references therein.

(iii) Even though in (2.4), we have used the notation $\Omega(t)$, our theory in this article is actually "infinitesimal" and the domain should be just Ω. The software platform LS-DYNA is capable of treating finite elasticity and, thus, the case of non-cylindrical or tubular domains $\Omega(t)$ (see, e.g., [28, 32]) by the use of *moving grids*.

In this paper, we see that the elastodynamic motion modes, based on the shapes of a horse and a camel can be related to the gaits of these two animals. We have tried to use modal analysis to determine the mode shapes, and then incorporate harmonic time dependence with these modes in order to understand their dynamic patterns and also possible biophysical interpretations. We have noticed that some computed modes are unrealistic and should be deemed spurious. There are also puzzling facts that, so far appear paradoxical such as Remark 3 has pointed out.

In the sequels, Parts II and III, we will continue the investigation along the same lines, for different animals. We hope we can broaden our understanding and obtain some answers.

Appendix: Frequencies of vibrations of the horse and camel

Table 2 The frequencies of modal analysis of, respectively, the horse and camel without floor or with floor. Note that the first 6 frequencies are actually zero (i.e., trivial). The rest 100 frequencies are nonzero. Therefore, we have included a total of 106 frequencies in the table

Freauencies(kHz)	Cases			
	Without floor		With floor	
	Horse	Camel	Horse	Camel
1	2.682837E−07	7.782041 E−08	5.960018E−07	8.870288E−08
2	2.698932E−07	8.501547E−08	6.376279E−07	9.029571 E−08
3	2.715966E−07	8.984321 E−08	7.967601 E−07	1.250446E−07
4	2.942210E−07	1.236262E−07	2.824282E−05	2.508591 E−05
5	3.048397E−07	1.385396E−07	4.985253E−05	2.591457E−05
6	3.262213 E−07	1.481239E−07	5.148981 E−05	3.027630E−05
7	3.612236E−05	1.988243E−05	5.958097E−05	3.043914E−05
8	3.746421E−05	2.116354E−05	6.165072E−05	3.050887E−05
9	3.981709E−05	2.197625E−05	6.609092E−05	3.468566E−05
10	4.470078E−05	2.238936E−05	7.337863E−05	3.471596E−05
11	4.716380E−05	2.296072E−05	7.544233 E−05	3.535281 E−05
12	4.728704E−05	2.531786E−05	8.186453 E−05	3.556314E−05
13	5.113975E−05	2.724082E−05	9.042398E−05	4.110963 E−05
14	5.411122E−05	2.846865E−05	9.247168E−05	4.778758E−05
15	5.533975E−05	4.168540E−05	9.346338E−05	5.328695E−05
16	7.541136E−05	4.514064E−05	9.593075E−05	5.354626E−05
17	1.074904E−04	5.369640E−05	1.166028E−04	5.660732E−05
18	1.292400E−04	5.404641 E−05	1.489392E−04	6.016764E−05
19	1.430821 E−04	7.404020E−05	1.632743 E−04	8.945863E−05
20	1.507188E−04	7.6043 70E−05	1.655328E−04	9.028651 E−05
21	1.806348E−04	8.083555E−05	1.846387E−04	9.573340E−05
22	1.824431 E−04	8.423719E−05	1.857892E−04	9.981593E−05
23	1.934547E−04	8.607738E−05	2.098809E−04	1.137995E−04
24	1.966530E−04	8.819308E−05	2.640247E−04	1.382627E−04
25	2.090820E−04	9.325324E−05	2.718732E−04	1.397781 E−04
26	2.308291 E−04	9.485306E−05	2.780743 E−04	1.539564E−04
27	2.322199E−04	1.136339E−04	3.018996E−04	1.550329E−04
28	2.523299E−04	1.192159E−04	3.205913E−04	1.636019E−04
29	2.548750E−04	1.204490E−04	3.312417E−04	1.646155E−04
30	2.826606E−04	1.441831 E−04	3.396648E−04	1.658929E−04
31	2.849240E−04	1.449194E−04	3.426114E−04	1.721582E−04
32	2.940045E−04	1.633624E−04	3.930962E−04	1.746178E−04
33	2.968315 E−04	1.653891E−04	4.064068E−04	1.777859E−04
34	3.202934E−04	1.806363E−04	4.073509E−04	2.311469E−04

Table 2 continued

Freauencies(kHz)	Cases			
	Without floor		With floor	
	Horse	Camel	Horse	Camel
35	3.326874E−04	1.811422E−04	4.134993 E−04	2.315879E−04
36	3.411629E−04	1.921651 E−04	4.322402E−04	2.460855E−04
37	3.642983E−04	1.954439E−04	4.829740E−04	2.591770E−04
38	3.807682E−04	2.324036E−04	4.849586E−04	2.684810E−04
39	4.187322E−04	2.330256E−04	4.904498E−04	2.884414E−04
40	4.494040E−04	2.398744E−04	5.000302E−04	2.891487E−04
41	4.668644E−04	2.411085E−04	5.734961 E−04	2.972601 E−04
42	4.693801 E−04	2.499352E−04	5.790548E−04	2.993720E−04
43	4.848566E−04	2.578354E−04	6.073742E−04	3.106098E−04
44	5.071372E−04	2.645231 E−04	6.354170E−04	3.116237E−04
45	5.197877E−04	2.805333E−04	6.458671 E−04	3.145439E−04
46	5.430603 E−04	2.838393E−04	6.550777E−04	3.244489E−04
47	5.613462E−04	2.933349E−04	6.601517E−04	3.431158E−04
48	5.654203 E−04	2.965207E−04	6.623351 E−04	3.454160E−04
49	5.682905E−04	2.981204E−04	6.932298E−04	3.486606E−04
50	5.839933E−04	3.0323 86E−04	7.220901 E−04	3.521011 E−04
51	6.174993 E−04	3.133389E−04	7.371502E−04	3.617396E−04
52	6.242691 E−04	3.139433E−04	7.536744E−04	3.819765E−04
53	6.546504E−04	3.320978E−04	7.673282E−04	4.047487E−04
54	6.613228E−04	3.414492E−04	7.907323E−04	4.069110E−04
55	6.877004E−04	3.457531 E−04	7.936365E−04	4.154980E−04
56	6.982786E−04	3.499769E−04	7.964884E−04	4.184556E−04
57	7.085598E−04	3.694328E−04	8.163194E−04	4.431713E−04
58	7.318584E−04	3.744884E−04	8.298294E−04	4.573863E−04
59	7.498630E−04	3.853117E−04	8.321392E−04	4.749502E−04
60	7.604048E−04	3.958726E−04	8.594311 E−04	4.825672E−04
61	7.743684E−04	4.073767E−04	8.920627E−04	5.028085E−04
62	7.854610E−04	4.151684E−04	9.027903E−04	5.091474E−04
63	7.942847E−04	4.213582E−04	9.240817E−04	5.116811E−04
64	8.071499E−04	4.322042E−04	9.351098E−04	5.255655E−04
65	8.093569E−04	4.431469E−04	9.582129E−04	5.292059E−04
66	8.510681E−04	4.466911 E−04	9.659081 E−04	5.346558E−04
67	8.618525E−04	4.739915E−04	9.965970E−04	5.503691 E−04
68	8.794260E−04	4.844556E−04	1.016364E−03	5.514565E−04
69	8.905136E−04	4.943253E−04	1.034318E−03	5.605775E−04
70	9.194891E−04	5.042767E−04	1.058526E−03	5.699902E−04
71	9.485025E−04	5.109038E−04	1.059480E−03	5.752574E−04

Table 2 continued

Freauencies(kHz)	Cases			
	Without floor		With floor	
	Horse	Camel	Horse	Camel
72	9.565653E−04	5.267613E−04	1.098479E−03	5.764628E−04
73	9.622925E−04	5.316049E−04	1.104805E−03	6.062658E−04
74	9.856625E−04	5.343943E−04	1.108293E−03	6.104055E−04
75	1.005030E−03	5.357071 E−04	1.118400E−03	6.117267E−04
76	1.011987E−03	5.588741 E−04	1.128361E−03	6.206276E−04
77	1.042086E−03	5.698325E−04	1.138594E−03	6.363081E−04
78	1.054168E−03	5.719594E−04	1.144335E−03	6.463295E−04
79	1.071218E−03	5.863935E−04	1.162788E−03	6.576478E−04
80	1.077019E−03	5.885098E−04	1.174661 E−03	6.579826E−04
81	1.110326E−03	6.059693E−04	1.182269E−03	6.668907E−04
82	1.117007E−03	6.1 1 1335E−04	1.189629E−03	6.719039E−04
83	1.120396E−03	6.254476E−04	1.221887E−03	6.886119E−04
84	1.123463E−03	6.392601 E−04	1.223834E−03	6.899093E−04
85	1.142500E−03	6.420590E−04	1.243257E−03	6.996813E−04
86	1.159416E−03	6.558190E−04	1.257744E−03	7.080962E−04
87	1.169230E−03	6.579580E−04	1.262451 E−03	7.157959E−04
88	1.183948E−03	6.755023E−04	1.290535E−03	7.251416E−04
89	1.192569E−03	6.769977E−04	1.297631 E−03	7.281561 E−04
90	1.224578E−03	6.870269E−04	1.300296E−03	7.485772E−04
91	1.247830E−03	6.895986E−04	1.328999E−03	7.499079E−04
92	1.248904E−03	6.899891 E−04	1.335338E−03	7.599794E−04
93	1.250932E−03	7.003730E−04	1.382327E−03	7.753743E−04
94	1.267440E−03	7.085183E−04	1.388511 E−03	7.823558E−04
95	1.268714E−03	7.126016E−04	1.416430E−03	7.951849E−04
96	1.277472E−03	7.139017E−04	1.428450E−03	8.084280E−04
97	1.295707E−03	7.271943E−04	1.434049E−03	8.137768E−04
98	1.315622E−03	7.357517E−04	1.451152E−03	8.212269E−04
99	1.332583E−03	7.447619E−04	1.451495E−03	8.258597E−04
100	1.339631E−03	7.488833E−04	1.468415E−03	8.312575E−04
101	1.351359E−03	7.705463E−04	1.469908E−03	8.488085E−04
102	1.380976E−03	7.822690E−04	1.474464E−03	8.599536E−04
103	1.395750E−03	7.926702E−04	1.493255E−03	8.606417E−04
104	1.403064E−03	8.045750E−04	1.520884E−03	8.671795E−04
105	1.420528E−03	8.251889E−04	1.524736E−03	8.893111 E−04
106	1.421298E−03	8.270509E−04	1.530157E−03	8.945109E−04

References

1. Kac, M.: Can one hear the shape of a drum? Am. Math. Mon. **73**(4P2), 1–23 (1966)
2. Gordon, C., Webb, D.L., Wolpert, S.: One cannot hear the shape of a drum. Bull. Am. Math. Soc. **27**(1), 134–138 (1992)
3. Zelditch, S.: Spectral determination of analytic bi-axisymmetric plane domains. Geom. Funct. Anal. **10**(3), 628–677 (2000)
4. Animals, see the website of Biology Online. https://www.biologyonline.com/dictionary/animal
5. Thompson, D.W., Thompson, D.W.: On Growth and Form, vol. 2. Cambridge University Press, Cambridge (1942)
6. Allometry. https://en.wikipedia.org/wiki/Allometry/
7. Vitalism. https://en.wikipedia.org/wiki/Vitalism/
8. Turing, A.M.: The chemical basis of morphogenesis. Bull. Math. Biol. **52**(1), 153–197 (1990)
9. Wu, J., Qiu, Y.: Modelling of seated human body exposed to combined vertical, lateral and roll vibrations. J. Sound Vib. **485**, 115509 (2020)
10. Yue, Z., Mester, J.: A modal analysis of resonance during the whole-body vibration. Stud. Appl. Math. **112**(3), 293–314 (2004)
11. van der Weele, J.P., Banning, E.J.: Mode interaction in horses, tea, and other nonlinear oscillators: the universal role of symmetry. Am. J. Phys. **69**(9), 953–965 (2001)
12. Banning, E., Van der Weele, J.: Mode competition in a system of two parametrically driven pendulums: the Hamiltonian case. Physica A **220**(3–4), 485–533 (1995)
13. Banning, E., Van der Weele, J., Ross, J., Kettenis, M.: Mode competition in a system of two parametrically driven pendulums with nonlinear coupling. Physica A **245**(1–2), 49–98 (1997)
14. Banning, E., Van der Weele, J., Ross, J., Kettenis, M., de Kleine, E.: Mode competition in a system of two parametrically driven pendulums; the dissipative case. Physica A **245**(1–2), 11–48 (1997)
15. Banning, E., Van der Weele, J., Kettenis, M.: Mode competition in a system of two parametrically driven pendulums; the role of symmetry. Physica A **247**(1–4), 281–311 (1997)
16. Van der Weele, J., Banning, E.: Mode interaction in a cup of coffee and other nonlinear oscillators. Nonlinear Phenom. Complex Syst. **3**(3), 268–283 (2000)
17. Chen, G., Scully, M.M., Huang, J., Sergeev, A., Yang, J., Wei, C.-Q., Monday, P., Cohen, L., Cheng, X.-G., Liu, S.-Y., Wang, J., Zhou, S.-Q.: Fundamental biomechanical modes of motion of the human body as human vibration
18. Ciarlet, P.G.: The Finite Element Method for Elliptic Problems. SIAM, Philadelphia (2002)
19. LSTC, LS-DYNA Theory Manual. https://ftp.lstc.com/anonymous/outgoing/jday/manuals/DRAFT_Theory.pdf/
20. Korn, A.: Solution générale du problème d'équilibre dans la théorie de l'élasticité, dans le cas ou les efforts sont donnés à la surface, Annales de la Faculté des sciences de Toulouse. Mathématiques **10**, 165–269 (1908)
21. Images of a thoroughbred. https://www.google.com/imgres?imghbreakurls=https%253A%252F%252Fwww.liveabout.com%252Fthmb%252FqntCirSxgk-xarPYt-rUJDyCk7Q%253D%252F1000x750%252Fsmart%252Ffilters%253Ano_upscale()%252Fsecretariat-hancock-56a4da855f9b58b7d0d98806.jpg&imgrefhbreakurls=https%253A%252F%252Fwww.liveabout
22. CAD horse model. https://blendermarket.com/products/horse-base-mesh
23. SolidWorks software package. https://my.solidworks.com/
24. ANSYS Geometry. https://grabcad.com/library?sort=most_downloaded&tags=ansys
25. Blender software (Home of the Blender project-Free and Open 3D artistic rendering and movie-making software platform). https://www.blender.org/
26. 3D Models. https://creazilla.com/nodes/3060-camel-3d-model/
27. LSTC, Contact Modeling in LS-DYNA. https://www.dynasupport.com/tutorial/ls-dyna-users-guide/contact-modeling-in-ls-dyna
28. Dziri, R.: Optimal tubes for non-cylindrical Navier–Stokes flows with Navier boundary condition. Evol. Equ. Control Theory **12**(3), 1014–1038 (2023)
29. Ganghoffer, J.-F., Plotnikov, P.I., Sokolowski, J.: Nonconvex model of material growth: mathematical theory. Arch. Ration. Mech. Anal. **230**, 839–910 (2018)
30. Plotnikov, P.I., Ganghoffer, J., Sokolowski, J.: Volumetric Material Growth: Mathematical Theory, Doklady Mathematics, vol. 94, pp. 498–501. Springer, Cham (2016)

31. Ganghoffer, J.-F., Plotnikov, P.I., Sokołowski, J.: Mathematical modeling of volumetric material growth in thermoelasticity. J. Elast. **117**, 111–138 (2014)
32. Moubachir, M., Zolesio, J.-P.: Moving Shape Analysis and Control: Applications to Fluid Structure Interactions. CRC Press, Boca Raton (2006)

Authors and Affiliations

Goong Chen[1,2,3] · Jingtong Huang[1] · Chunqiu Wei[4] · Jing Yang[5] · Matthew M. Scully[1] · Alexey Sergeev[1] · Ming-Chieh Chen[6] · Steven G. Krantz[7] · Pengfei Yao[8,9] · Tiexin Guo[10] · Junmin Wang[5]

[1]   Department of Mathematics, Texas A&M University, College Station, TX 77843, USA

[2]   Institute for Quantum Science and Engineering, Texas A&M University, College Station, TX 77843, USA

[3]   National Center for Theoretical Sciences, National Tsing Hua University, Hsinchu Branch, Hsinchu, Taiwan, R.O.C.

[4]   Department of Mathematics and Data Science, Beijing University of Civil Engineering and Architecture, Beijing 100044, China

[5]   School of Mathematics, Beijing Institute of Technology, Beijing 100081, China

[6]   Department of Mechanical Engineering, Cheng Shiu University, Kaohsiung 83347, Taiwan, R.O.C.

[7]   Department of Mathematics, Washington University at St. Louis, St. Louis, MO 63130, USA

[8]   Key Laboratory of Complex Systems and Data Science of Ministry of Education, School of Mathematics Shanxi University, Taiyuan 030006, Shanxi, China

[9]   Institute of Systems Science Academy of Mathematics and Systems Science, Academia Sinica, Beijing 100190, China

[10] School of Mathematics and Statistics, Central South University, Changsha 410083, Hunan, China